Analysis of the impact of sedimentological heterogeneity and fractures on fluid flow properties in a deltaic reservoir setting using numerical models

By

Martin Peter Lipus

In partial fulfilment of the requirements for the degree of

Master of Science

In Petroleum Engineering and Geosciences

at Delft University of Technology,

to be defended publicly on Monday August 31, 2015 at 15:00.

Supervisor:	Dr. J.E.A. Storms
Thesis committee:	Dr. N.J. Hardebol
	H. van der Vegt
	Dr. A. Barnhoorn

An electronic version of this thesis is available at http://repository.tudelft.nl/

Acknowledgements

Over the past months I had the chance to investigate a fascinating research topic in the scope of my MSc thesis at Delft University of Technology. This project represents the end of two fantastic years as a master's student in Delft. I would like to thank all the people inside and outside the campus which I have met over the time here in the Netherlands.

Starting with the people outside the university, I would like to thank my flat mates in *CafeTwee* from whom I have learnt a lot about the dutch culture, history and traditions as well as the dutch language. I would also like to thank my team members from *FC Suriname United* for two great seasons in the *maandag competitie* which made Monday surely the best day of the week. I am also grateful for all the people I have met during the MSc program "Petroleum Engineering and Geoscienes".

From people that were involved in this study, I would like to thank my thesis supervisor Joep Storms for his guidance and support during the whole time of the project. I also would like to thank Nico Hardebol whose knowledge on the field of structural geology and forward numerical modelling was of great importance for my work. I find that my thesis meetings were always very productive and interesting. I especially enjoyed how well the communication worked between all persons involved.

A special thanks goes to the third person of my thesis committee, Helena van der Vegt, who I heartily thank for her constant guidance, sharing of technical expertise with the setup of Delft3D models, productive discussions we had and helping to improve the structure of the report. Without her assistance the completion of this project would not be possible in the given time frame.

I would also like to thank my mother and father for their support throughout the years of my study as well as my girlfriend Caro for all the encouraging high definition Skype conversation we had over the last weeks although they crashed after five minutes every time.

Finally, I would like to thank the PhD students from room 03.120 for integrating me into their lively and friendly work environment and for providing me unlimited access to a whole range of caffeine-rich beverages.

Delft, 24 August 2015

Martin Lipus

Abstract

Process-based numerical simulations in river delta modelling have demonstrated the importance of hydraulic and sedimentary forcing mechanisms on delta morphodynamics. Insights of these simulations on deltaic systems have a high potential to improve reservoir predictions in the industry. However, detailed morphological studies are typically conducted in a qualitative manner which provides unsatisfactory results for reservoir characterisations. This work presents a systematic workflow to perform semi-quantitative classification of process-based deltaic models created in Delft3D-FLOW with the use of dynamic reservoir flow models. The flow response of synthetic reservoir models is investigated using two Delft3D models which were modelled with varying sediment input conditions. Subdomains of the models were extracted and stacked onto each other to model sequence stratigraphic stacking pattern such as progradation, aggradation and retrogradation. Moreover, the effect of different orientations of production-injection well doublet and mechanical unit-confined fractures is investigated. As a proof of concept, a case study is conducted using 48 flow simulations. The results are investigated in terms of flow rates of the oil and water phase at the production well over time which is subsequently compared to average permeability maps of each individual parasequences. The findings are compared to sweep efficiencies per layer at the end of the flow simulation. Compared to finer sediment input compositions, the results suggest that coarser grained sediment input requires a lower pressure differential between injection and production well due to higher permeabilites but also a higher chance of quick water-breakthrough through a single parasequence. Furthermore, it was demonstrated that progradational stacking pattern result in a succession of parasequences with a higher area of incision compared to retrogradational stacking pattern which lead to improved vertical connectivity. The results show that the effect on the flow performance of the synthetic reservoir model is influenced stronger by the local occurrence of channels at the well location than the general stacking pattern. The results also indicate that fractures lead to higher differences in sweep efficiencies of individual parasequences, in particular when the fractures are orientated perpendicular to the main stream direction of the geological deposits. The work does not aim to present conclusive reservoir classification but should motivate other researchers to use the developed workflow for further quantitative reservoir analysis of Delft3D models.

Contents

List of Figures

List of tables

1. Introduction

1.1. Problem statement and objective

Creating reliable reservoir property predictions of deposits of deltaic origin is of great importance for the hydrocarbon industry. Approximately 30% of the global oil and gas reserves are located in deltaic deposits (Tyler & Finley, 1991). Sedimentary succession in such systems shows a high variability both in a vertical as well as in lateral directions due to the limited extent of the geometries of depositional facies. In terms of production characteristics these deposits can show highly variable sand body connectivity and tortuous flow paths. Therefore hydrocarbon field operators typically face problems such as pressure compartmentalization, poor sweep efficiency and early water-break through (Farrell & Abreu, 2006). On top of that, the flow behaviour of sedimentary bodies can be altered by local fractures that may or may not connect sand bodies across fine-grained flow baffles. With the help of reservoir models it is possible to capture the complex interplay of sedimentology and stratigraphy with post-depositional structuration. However, three-dimensional depositional models of reservoirs are commonly simplified approximations because of lacking data or restrictions by the model resolution. These simplifications often lead to neglect of key heterogeneities such as impermeable flow baffles or thief zones.

A rather young and promising technique is provided by process-based numerical models which generate high resolution 3D stratigraphy. Until today, a lot of effort was invested to understand the relative importance of controlling factors such as hydraulic forcing of river, wave and tide on the morphology and architectural elements of deltas. The analysis of the numerical data has elucidated the key factors controlling deltas. These studies have shown how sensitive the formation of a delta complex reacts to varying boundary conditions. From a view point of a field operator however, this knowledge is only of limited applicability. For practical reasons it would be much more insightful to gain knowledge of the consequences of different delta types in terms of on the expected production life-time or connectivity of different layers in the subsurface. Not only should it be investigated how the flow migrates through different delta models but also how a stack of delta sequences behaves in a varying sequence stratigraphic framework. In order to bridge the gap between morphodynamic-stratigraphic and dynamic flow models, the following research questions are addressed:

What is the effect of delta vertical stratigraphy / stacking patterns on reservoir connectivity and the role of fracture permeability enhancement?

The research question was addressed by means of process-based geological models using Delft3D. Once a workflow was established to address this research question a case study was conducted on different realisations of synthetic reservoir models. This case study addresses on the following questions:

How is the flow response of synthetic reservoir models affected by the

1) *sediment composition of the delta?*
2) *sequence stratigraphic stacking pattern?*
3) *orientation of a production-injection well pair?*
4) *occurrence of unit-confined fractures and their orientation?*

1.2. General workflow and scope

This study establishes a workflow to create process based geological reservoir models using Delft3D. With the developed programming scripts and documentation a workflow is created for researchers to quantitatively investigate the reservoir flow performance of Delft3D models in a sequence stratigraphic context. Additionally, mechanical stratigraphic controls are developed that enable the implementation of a mechanical unit confined fracture network which can be integrated in the flow simulation. A total number of 48 simulation runs were conducted to verify the practicability of the developed workflow. A schematic flow chart of the workflow is presented in Figure 1.

This study begins with the numerical simulation of different realisations of deltaic systems in Delft3D (Deltares, 2011). The generated model was subsequently loaded into MATLAB (The Mathworks Inc., MATLAB Version R2014b) where a script was developed to create a vertical stack of multiple pieces of the Delft3D model (parasequence) in order to generate a synthetic reservoir
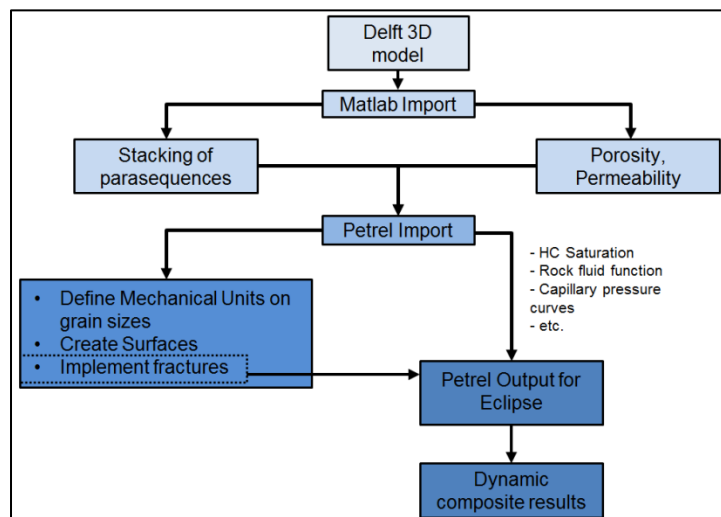
Figure 1: Schematic workflow of this study

model with a sequence stratigraphic context. The resulting model was then integrated into the reservoir simulation package PETREL (SCHLUMBERGER, Petrel E&P Software Platform Version 2013.8, 2015). After having defined reservoir parameters and locations of

10

injection and production wells, simulations are conducted in order to quantify the heterogeneity and sweep efficiency of the sythetic reservoir models. The flow simulations ran with the ECLIPSE simulator (SCHLUMBERGER, ECLIPSE Reference Manual Version 2013.2, Technical Description, 2013) were afterwards repeated with fractured synthetic reservoir models which were modeled with unit confined fractures.

The results successfully give an insight in the effect of delta morphology, stratigraphy and fracture stratigraphy on the flow performance of deltaic deposits. Since carrying out simulations was only possible in a limited time frame, the results should be regarded as a proof of feasibility rather than a conclusive reservoir classification. Further reservoir simulations are needed to create more certain reservoir predictions. The potential and improvements of this methodology are discussed in the last part.

2. Sedimentary deposition in deltaic settings

Overview of fluviatile coastlines and their economic value

Sandy, channelized deltaic systems deposit sediment at the termination of rivers at the shorelines of standing water bodies (e.g. oceans, lakes). As rivers approaches the margin of the basin it increases in cross-sectional view in both width and depth. Therefore the channel area perpendicular to the flow increases while the flow rate remains constant which leads to a rapid seaward deceleration and deposition of sediments. Typically, these deposits form a basin-ward-thinning wedge which progrades sea-wards over time. The major controls on accommodation space are changes in the relative sea level which is the product of eustatic- and tectonic movement. Depending on the balance between created accommodation space and sediment supply, deltaic systems can vary greatly in the geological record. In some areas in the world (e.g. Mississippi delta in the northern Gulf of Mexico) sediment accumulation rates can become extremely high when both sediment input as well as tectonic subsidence is high. These large scale sedimentary bodies received vast attention from the energy industry for many centuries. Although deltaic systems can show a high divergence in shape and spatial dimension (as later explained) they often share attributes which makes them very interesting as hydrocarbon plays. That is because in a deltaic setting usually the four key ingredients, namely source rock, reservoir rock, seal and trap, are present to form a petroleum system (Leeder, 1999).

2.1. Evolution of deltas

The morphology and facies distribution of a delta is governed by various factors (see Figure 2). The fluvial regime which brings the sediment into the system from the landward highlands as well as the basinal regime (e.g. wind and waves) controls the evolution of a deltaic system. Since there are multiple variables involved in the determination of the morphology and the evolution of a delta it is only of limited applicability to determine to which degree each individual factor is contribution to the final deposit. (Orton & Reading, 1993). Different than other depositional environments, deltas defy a simple sedimentary model as for example applicable for the distinction of different fluvial deposits such as meandering and braided river systems or aeolian deposits such as dunes.
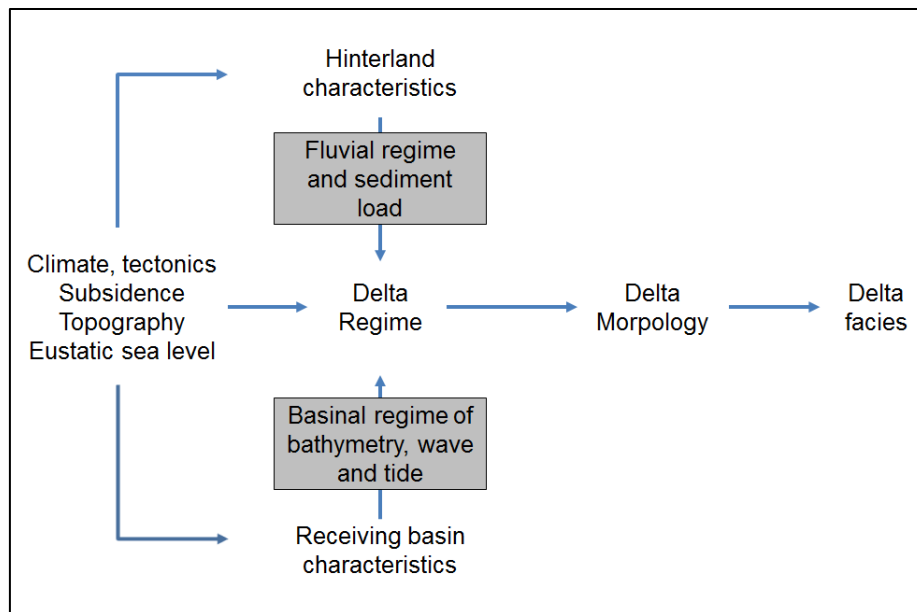
Figure 2: Factors affecting delta morphology and facies distribution (after (Postma, 1990))

Delta Geometry

The letter *Delta* (Δ) implies the general shape of a deltaic system assuming the paleoflow direction is orientated perpendicular to the coastline. The narrow tip is situated at the location where the distributary channel enters the basin and deposits spread onto the shelf and are exposed to the hydraulic forces as explained earlier. Many possibilities exist as to how to define sedimentary facies in a deltaic setting. Depending on the scale, conceptual models of deltas presented in literature can either be simple and display the main domains (km scale) or become very detailed at bed scale. However, what all these models have in common is that the delta is fed by a laterally bounded distributary channel with or without levee deposits at the flanks which disperses onto a shelf in a network of individual channels. As the flow velocity decreases, coarse grained sediments get deposited at the end of the channels (stream mouth bar). Moving radially from the river input sedimentary deposits decrease in grain size. Facies description such as proximal delta front and distal delta front is often used to describe the deltas morphology. The most distal part of a delta is defined as the prodelta where predominantly silts are deposited.

2.2. Delta Classification

Various studies on finding generalised methods to classify deltaic systems are given in the literature (Wright & Coleman, 1973) and (Komar, 1973). Galloway realised that a way to classify deltas is given by their main hydraulic parameter that led to their deposition. According to him, the three main factors which govern the appearance of a delta are the river discharge (and discharge variability), wave energy and tidal range. The approach results in a ternary diagram for deltaic systems with the end-members "river-dominated", "wave-dominated" and "tide-dominated" deltas (Galloway W. G., 1975). His idea was later further developed by Orton and Reading who realized that additionally the average grain size of the sediment plays a vital role in the morphological evolution of the delta (see Figure 3). They also discussed the effect of grain size on the gradient and channel morphology on the delta plain, the type of shoreline, the interaction between river sediments and saline basinal waters at the mouth bar, deformation and re-sedimentation (Orton & Reading, 1993). In their work they gathered data from a total number of 37 existing deltas from all over the world in terms of discharge, sediment load and particle size, slope gradient and wave and tidal range. Schematic drawings from 10 large deltas are categorized in Figure 3.
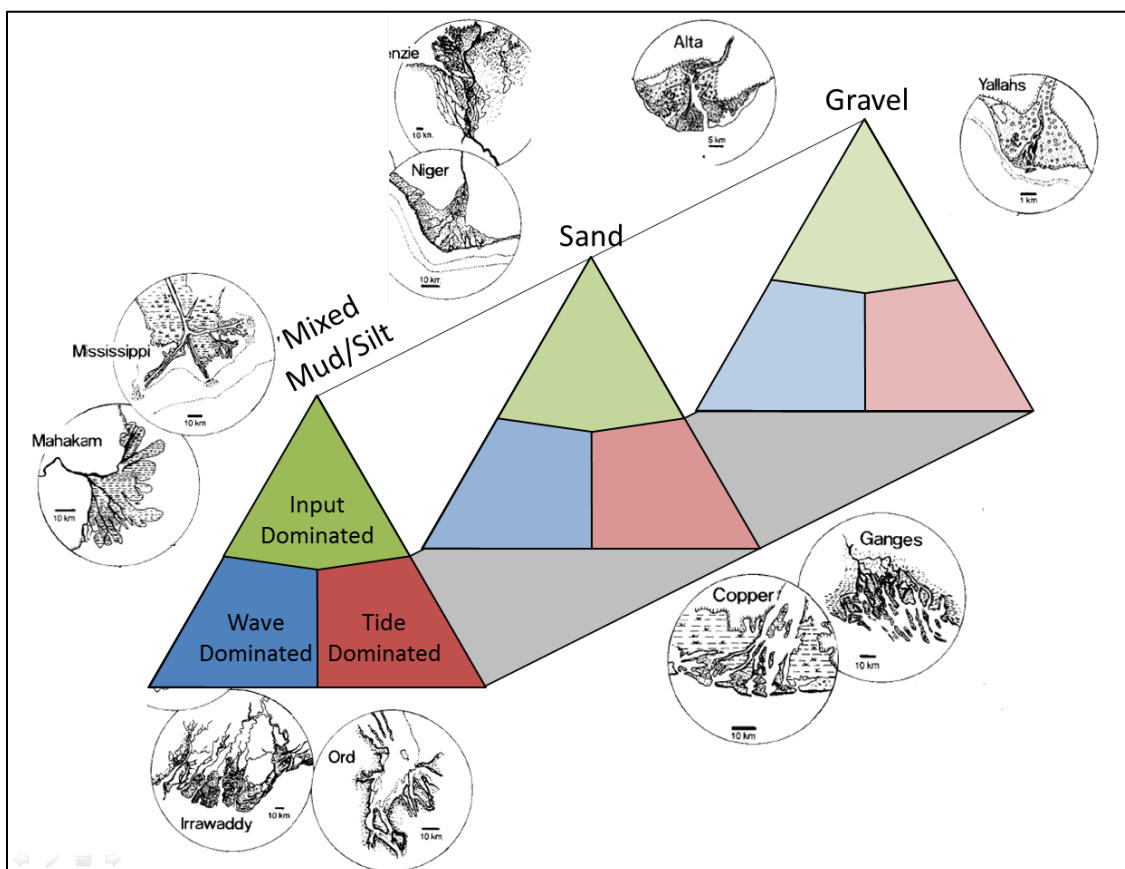
Figure 3: Delta classification ternary diagram based on hydraulic parameters and prevailing grain size feeding the system (modified from (Orton & Reading, 1993))

14

Another study focuses on the prediction of process dominance at the coastline for ancient depositional systems by including the basin shape, costal morphology, accommodation space, sediment supply and shoreline trajectory for the classification of deltas (Ainsworth et al., 2011). The result was a decision tree which provides a predictive tool for the coastal process dominance. It includes the relative dominance of each of the three end members of Galloways ternary diagram (fluvial, wave and tidal resonance). Additionally, a distinction is made between high accommodation space/ sediment supply (A/S) ratio and low A/S ratio systems and the type of shoreline morphology with the three classes straight to lobate, moderately embayed or highly embayed. The outcome of the decision tree is a one to three letter code that comprises the relative dominance of fluvial, wave and tide forcing. What is unique about their approach is that it combines the potential outcome of the delta geometries with knowledge that has been gained from non-fluviatile coastlines. Depending whether the system has been deposited in a transgressive or regressive phase, different facies might be deposited. With the integration of the sequence stratigraphic trend it is possible to quantify the likelihood of certain costal facies to occur. In a regressive setting for example, preferably strand plains, cheniers and tidal flats form whereas in a transgressive settings, estuaries and barrier island form (see Figure 4). This approach can help improving prediction of the subsurface geometries of a given ancient delta.
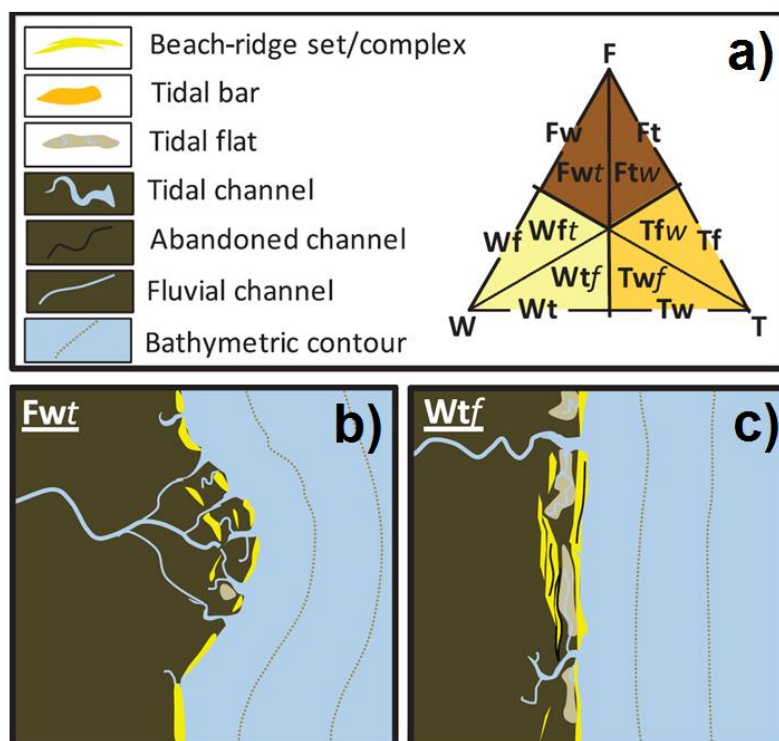
Figure 4: a) Costal process classification ternary plots with 15 classification categories. b) and c) show schematic plan view drawings of two realisations. b) Fwt – Fluvial dominated, wave secondary and low tidal forcing. C) Wtf – Wave dominated, tidal secondary and little fluvial forcing. In Ainsworth et al., 2011 modified from Galloway W. G., 1975

In order to apply this concept to an ancient coastal deposit which is located in subsurface and to draw conclusions from it, it is logically necessary to obtain data from the reservoir and integrate it into the decision tree. The result of their work gives a practical differentiation of accommodation space / sediment supply ratio (A/S ratios) by looking at well logs and cores (see Figure 5). In their approach they have determined a ratio of the total thickness of one individual parasequence (T_h) divided by the sand to shale ratio (S/S_h) over the same interval. If for example a parasequence has a thickness of $T_h = 10m$ and a high sand to shale ratio of $S/S_h = 3$, the resulting ratio becomes low ($T_h/(S/S_h) = 3.33$). On the other side, with the same parasequence thickness and a low sand to shale ratio of $S/S_h = 0.3$, the ratio becomes high ($T_h/(S/S_h) = 30$). Ainsworth and his colleagues used this concept to define ratios which correspond to a low A/S ratio (where $T_h/(S/S_h) < 10$) and high A/S ratio (where $T_h/(S/S_h) > 10$). These distinctions are then used to assess the systems tract of each individual parasequence. As explained in their work, the concept generates only indicative results. Further work is required to create a finer and more reliable distinction of the prognosticated systems tracts. However, this method of assessing the sequence stratigraphic framework is applicable for the implementation of the geological flow models that are created in this study.
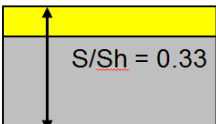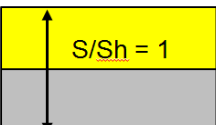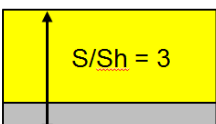
Figure 5: Accommodation/sediment supply (A/S) ratio obtained from the ratio of total thickness of a parasequence divided by its sand/shale ratio (modified from Ainsworth et al., 2011)

2.3. Stratigraphic architecture

Delta lobes are rather thin bedded deposits usually in the range of several meters in thickness. When dealing with a deltaic reservoir it can easily reach a couple of hundreds of meters. That is because multiple sequences of delta lobes are stacked onto each other over time. These stacks can partly be well connected through erosion, reworking and incision of sequential parasequences or isolated from each other by impermeable flow baffles.

As explained before, a delta lobe progrades onto the shelf as long as the channels that feeds the lobe is active. Once the feeding channel becomes inactive at the position of the lobe no further sediments from fluvial origin arrive at the lobe and deposition continues at a different location. The lobe is now exposed to the sea and will be altered by the currents, tides and waves to varying degrees, depending on the environment of deposition. Depending on the climate, vegetation can assist in stabilizing and preserving the initial shape of the lobe. Where subsidence rates of a sedimentary basin are high the lobe can also be preserved by quick deepening. Finer grained silty to muddy deposits subsequently cover these lobes. An example of a basin with an extremely high subsidence rate is the deltaic deposits in the northern Gulf of Mexico where the Mississippi delta is located. The high subsidence rate in combination with high sediment flux led to deltaic deposits of a total thickness of approximately 2 km from the Lower Miocene until today (Galloway, 2008). On that macroscopic basin-wide level clear boundaries are defined in the geological record that represent for example aggradational phases or progradational phases of the delta.

On this large scale it is possible to characterize the stacking pattern of the deltaic deposits using conventional sequence stratigraphic terms and systems tracts. On a smaller scale of individual parasequences this terminology can only be partly applied (Van Wagoner et al., 1990). Stacking pattern of individual delta lobes is governed by the point source of the feeder channel. Over time the depo-centre changes both orientation and location. So even if on the large scale a delta system is prograding onto a shelf, it does not mean that the lobes prograde symmetrically. There might be certain delta lobes that suggest a contrary stacking pattern due to local non-deposition. There are two different processes active that control the stratigraphy of deltas. Delta lobe switching in a radial sense from the fluvial inlet is controlled by autogenic behaviour of channel avulsion. In contrast, the deposition along the axis in the offshore is governed by allogenic control factors such as relative sea level rise and sediment supply (Wellner, 2005). Field studies have shown that the autogenic behaviour of deltaic systems can result in an offset of direction of deposition of two successive delta lobes in an angle as high as 90˚ in both clockwise and anticlockwise direction (Deveugle et al, 2011).

Van Wagoner et al. (1990) further stated that parasequences, which consist of relatively conformable successions of strata bound above and below by flooding surfaces, are the building blocks of unconformity-bounded sequences. These flooding surfaces are the key to interpret parasequences and they are recognized in the geological record by the juxtaposition of more basin-ward facies above more sea-ward facies. In cores flooding surfaces can be recognized as hummocky cross-bedded, upper-shoreface deposits overlain by rippled siltstones and mudstones which represent shelf deposition. Therefore a flooding surface would be represented in a well as a vertical transition from sandier facies overlain by muddier facies. When applying this definition of parasequences, one has to make sure that the muddier facies is not a shallow water deposit such as in a lagoon or a coastal plain mudstone. That would lead to a wrong characterisation of a reservoir since these muddy deposits have less lateral continuity compared to flooding surfaces. The different mud layers can either be distinguished by depositional structures, if cores are available, or by well-log signature and well correlations, if wire line logs are available (Larue & Legarre, 2004). When a number of parasequences are defined in a reservoir they can be grouped into sets with i.e. a progradational or retrogradational stacking trend. The stacking trend is often supported by studies about the shoreline geometry over time.

Despite the fact that the sequence stratigraphic terminology is not unambiguous to describe stacking patterns over a number of parasequences because of dynamics of deltaic system, this study uses these terms to describe stacking patterns of the synthetic deltaic reservoir models created in this study. Doing so, it is possible to quantify the effect of stacking trend on the vertical reservoir connectivity on a small scale of several individual parasequences.

2.4. Origin and formation of unit confined fractures

The role of delta stacking patterns and their effect on reservoir connectivity is the core work of this study. It is augmented by the inclusion of fractures that can achieve vertical cross-connections of sandstone bodies which are otherwise disconnected. It is well known that the physical properties of reservoirs are highly influenced by the distributed fracture field. Fractures can lead to enhanced permeabilites of reservoirs in case of open fractures and result in a higher vertical connectivity between adjacent layers. However, fractures can also lead to compartmentalisation due to cementation of fractures which eventually leads to a lower vertical connectivity. This study focuses on the role of fractures as fluid conduit and testing their role to breech low permeable shale layers and thus connect sandstone bodies in the deltaic sequence.

Since the fracture network can alternate the physical properties of a reservoir greatly it is of high importance to estimate their characteristics in real reservoir with the highest confidence possible. Normally the fracture model is predicted from data which is obtained from well logs. This hard data may give high certainty about the fracture network in vicinity of the well bore but when it comes to the extrapolation between a pair of wells the technique is biased by high uncertainty (Parney & LaPointe, 2002). A way to deal with this uncertainty was developed throughout an innovative method that subdivides outcropping stratigraphy into mechanical units (Bertotti et al., 2007). By studying a number of highly fractured outcrops and quantifying parameters such as the number of fractures, their specific orientation and their aperture along the vertical profile of the outcrops, they were able to relate the fracture pattern to the stratigraphy from which an objective method was developed by which the stratigraphy was subdivided into mechanical units. The statistical parameters obtained can then be translated into fracture intensities and spacing distances.

A fracture is any semi-planar discontinuity in a geologic formation along which deformation by opening or slip has occurred. Based on their genesis mechanism two main types of fractures are defined in relation with the strain effects: shear fractures called faults and extension fractures called joints. However, from a viewpoint of a reservoir engineer a distinction is rather made on the impact of the fractures on the flow than mechanical concepts. When describing the fracture network of a reservoir usually large scale fractures (from seismic survey) are distinguished from small-scale diffusive along individual reservoir layers.

Over the last decades, numerous studies were dedicated to the characteristics of opening-mode fractures in layered sedimentary rocks (e.g. (Cooke & Underwood, 2001) (Laubach et al., 2009)). Their work resulted in the acknowledgement that opening-fractures are confined to mechanical layers and that the fracture density is a function of both the mechanical property of the formation as well as the layer thickness (see Figure 6). Outcrop studies have shown that fractures primarily form along brittle rocks and often terminated at the top and the base of the mechanical rigid layer if it is surrounded by a ductile material, such as a shale layer (Cooke et al., 2006). Depending on their quantity, orientation and properties, these fractures can lead to significantly alternated flow behaviour in terms of its reservoir condition. In unit confined fractures the flow can preferably move through the fracture induced pathways leading to an early water breakthrough of an injection-production well doublet or to an increase of the natural sweep if the fractures connect isolated deposits to the main fluid path way.

When applying this knowledge to a reservoir model it is not applicable to model all fractures explicitly since the number of fractures in a rock volume can be very large. Therefore, it is necessary to create a model for the fracturing which can be implemented in a reservoir analysis. Statistical Discrete Fracture Network (DFN) models are used in this study in order to implement mechanical unit confined fractures to the synthetic reservoir models. Various studies have shown the capability of these mathematical models to capture most fracture patterns in terms of fracture orientation, size distribution, intensity, transmissivity and aperture (e.g. Dershowitz et al., 1998).
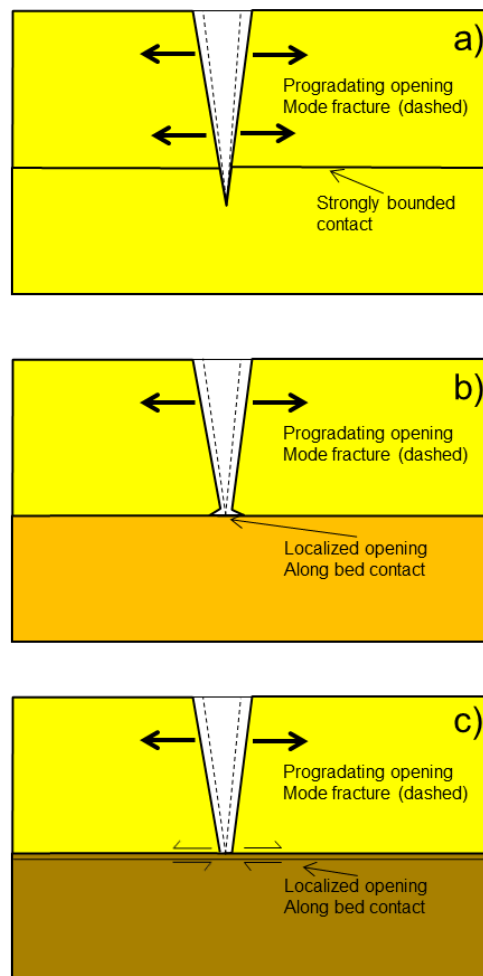
Figure 6: Postulated mechanisms for fracture progradation through and bounded by a bedding contact. A) fracture progradation through well bounded mechanically homogenous layers, b) fracture termination at bedding contact due to weak bonding, c) fracture termination due to slip along the bedding surface (modified from Cooke & Underwood, 2001)

3. Methodology

To evaluate the effect of sedimentological input parameters, the sequence stratigraphic regime and the effect of unit confined fractures on reservoir properties, this study performs numerical experiments on the response of dynamic flow simulations of process-based deltaic deposits. Therefore, flow characteristics of a range of deltaic deposits are investigated by generating a workflow to create 8 synthetic geological models which were subsequently subjected to 6 flow simulation each, 3 in a stream-wise and 3 in a span-wise injector-producer well pair orientation (see Figure 7). Two deltaic Delft3D-FLOW models with varying input conditions were created, each with three different stacking patterns (progradation, retrogradation & aggradation) to make up 6 synthetic geological models. The last two geological models use one of the 6 previously created synthetic models (Delft3D model: '25% sand' stacking pattern: retrogradational) and additionally contain unit confined fractures with two different fracture orientations.

Delft 3D Model	Stacking pattern	Well orientation with respect to coastline		Simulation No.
D3D model: '25% sand'	Retrogradational	Parallel to coastline		1 2 3
		Perpendicular to coastline		4 5 6
	Aggradational	Parallel to coastline		7 8 9
		Perpendicular to coastline		10 11 12
	Progradational	Parallel to coastline		13 14 15
		Perpendicular to coastline		16 17 18
D3D model: '35% sand'	Retrogradational		...	19 20 21
				22 23 24
	Aggradational		...	25 26 27
				28 29 30
	Progradational		...	31 32 33
				34 35 36
Fracture Study				
D3D model: '25% sand' Stacking pattern: 'Retrogradational'	Fractures parallel to coastline		...	37 38 39
				40 41 42
	Fractures perpendicular to coastline		...	43 44 45
				46 47 48

Figure 7: Overview of simulations runs of this study

3.1. Delft3D models design

Different than delta classification schemes developed from (Galloway W. G., 1975) and (Orton & Reading, 1993) which characterized deltas based on their final appearance, the approach of process-based Delft3D-FLOW models opens a world of a whole new understanding of the interplay of factors is that lead to the formation of architectural elements such as the periodical driving forces.

Delft3D is an open-source software suite which is developed by the independent institute for applied research Deltares. The software suite is composed of several modules which form a multidisciplinary approach for the generation of multidimensional (2D or 3D) physics-based models. Initially, it was intended for simulations in costal, river and estuarine areas. Deltares and the Delft3D community developed modules which make it possible to carry out simulation which account for water flow, sediment transports, waves, water quality, morphological developments and ecology (Deltares, 2011). The focus of this work includes simulation with changing hydrodynamic boundary conditions and resulting sediment transport. The module which accounts for these processes is called Delft3D-FLOW. All models which are used in this study are generated using this module.
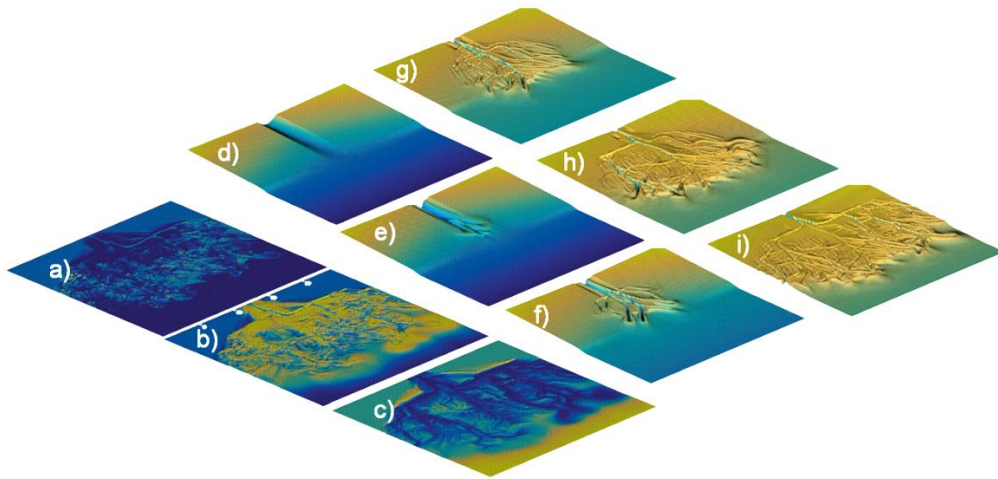
Figure 8: Example of a Delft3D model. a)-c) show the distribution of a grain fraction per layer. d)-i) show an example of the formation of a Delft3D model over time.

Various studies have been conducted in the last years which demonstrated the ability of morphodynamic-stratigraphic modelling of river-dominated deltaic setting with Delft3D-FLOW (e.g. Geleynse et al., 2010). The outcomes of these high resolution physics based models consist of river delta distributary networks as they can also are also observed in field observations. The authors have hypothesized that the cyclicity in driving forces such as the tides and annual discharge variances have a strong coupling to stratal patterns in deltas.

Moreover, they have concluded from the analysis of their delta simulations that the sediment input at the feeder channel has a strong control on the morphodynamics of the channels. The delta simulations which were run with a higher percentage of finer grained (cohesive) material tend to form single channel rivers with a high depth compared to simulations that were run with coarser sediment input. The higher cohesive material leads to more persistent sinuous channels which sweep across the delta floodplain. The coarser grained (non-cohesive) input results in multiple relatively shallow channels. This observation is in agreement with observations that were made in the nature (Makaske, 2001). Other authors confirm the observations from an analysis of 33 Delft3D models, that an increasing median grain size and therefore a decrease in cohesive sediment have the tendency to transform from elongated deltas with few channels towards semi-circular deltas with many channels (Caldwell & Edmonds, 2013).

Another study on the effect of grain size on deltaic morphologies concluded that finer sediment input results in a poor sand body connectivity and more bird-foot like morphology of the distributary channels (Slingerland et al., 2012). The coastline of these deltas is therefore more rugose. For the fine grained model they used a D50 median grain size of 12 µm. From the coarse grained model (D50 = 1000 µm) they concluded that a delta forms with a higher number of distributary channels and a rather fan-like plan form shape.

In order to run a Delft3D-FLOW (Version 4.00.01) (Deltares, 2011) simulation several steps are required such as the definition of the initial numerical grid, the bathymetry, boundary conditions and various physical and numerical parameters. The model setup is explained in this chapter. A detailed description of the numerical procedure of Delft3D is given in the literature (Geleynse, 2013).

Grid

The dimensions of the Delft3D models are 500 grid cells in stream-wise (X-axis) and 600 in the span-wise (Y-axis) direction. The grid cell size is 50 x 50 m leading to a total model domain of 25 x 30 km (see Figure 9). Total number of grid cells in the model is therefore 3 x10^5. The size of the grid was selected in a way that a balance is reached between capturing depositional facies with enough detail and to run the models in an acceptable simulation time.

Bathymetry

The initial bathymetry of the basin consists of an inlet on the left side from which the fluvial channel belt enters the basin. The fluvial inlet is 900 m in diameter with a convex shape and a maximum depth of 4 m in the centre of the channel. Towards the sea line, the channel belt

widens, creating a trough-like shape. The most distal area of the model the shelf break is modelled by a high slope of the sea floor leading to a significant deepening of the bathymetry. By doing so, the models tend to run more stable and less numerical errors occur during the simulation. The sea floor deepens constantly and rather shallow towards the distal area with 1 m for each 1330 m. At the flanks of the river inlet the topography increases to a height of 8 m above sea level. By doing so it is secured that the tidal influence induced by the sea does not lead to numerical errors at the side of the inlet.
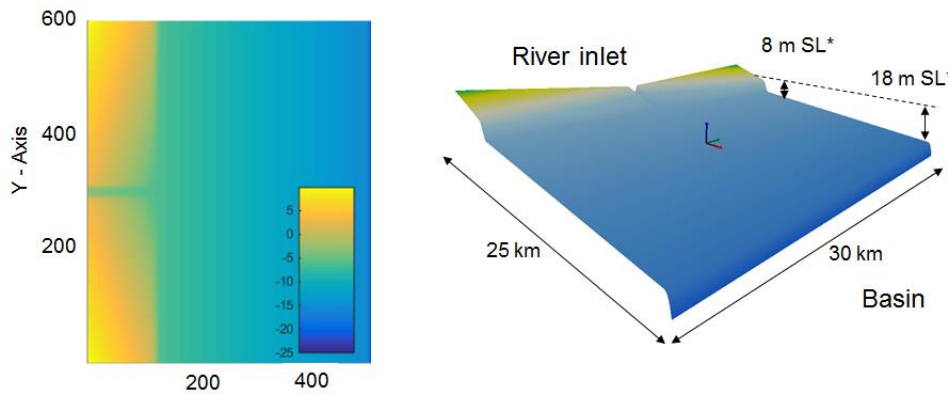
Figure 9: Model dimension and bathemetry used to run the Delft3D models

Boundary conditions

At the boundaries of the model domain boundary conditions are necessary in order to solve the hydrodynamic and morphodynamic equations in Delft3D. These boundaries simulate the influence of the area beyond the model or in other words the outer world.

The boundaries at the northern and southern side of the model domain are defined with the Neumann boundary condition. This condition is used to impose the alongshore water level gradient which should be applied to cross-shore boundaries (Deltares, 2011). The basin side on the right is assigned a water level constraint simulating a varying tidal signal. A constant harmonic tide has been defined for all models used in the simulation (see Table 1). The Delft3D-FLOW simulation enables the user to define various parameters regarding the hydrodynamic behaviour of the system. These values have been kept constant.

Table 1: Input parameters for the tidal influence

Frequency [deg/h]	0	13.9	15.0	28.8	30.0
Amplitude [m]	0	0.164	0.221	0.699	0.465
Phase [deg]	0	130.36	159.02	276.88	322.56

At the boundary of the 'river inlet' the flow rate is constant during the entire simulation at a discharge of 3000 m³/s. Two different Delft3D models are run at different sediment

compositions. In the summation both of the river inlets transport 100g of sediment into the basin with each 1 m³ of the discharge. The differences of the two models with respect to the sediment composition of the fluvial system are noted below (see Table 2). Five different sediment classes are used in this work to create a high resolution representation of the sediment composition in the different architectural elements of the delta model. The first model runs with a fluvial system that feeds the basin with rather fine material whereas the second model shows a realization of coarser grained sand dominated fluvial input. The sediment composition is captured in fractions for particular grain size mean diameter (D50).

Table 2: Definition of fluvial input in the two Delft3D models used for this study

Type of Sediment	Medium -fine sand	Fine - very fine sand	Very fine sand	Silt	Clay
D50: mean grain size	250 µm	150 µm	100 µm	17 µm	4 µm
	[g/m³]	[g/m³]	[g/m³]	[g/m³]	[g/m³]
Delta 1: '25% sand delta'	4	8	13	50	25
Delta 2: '35% sand delta'	6	12	17	48	17

Physical and numerical parameters

As mentioned earlier, the physical parameters are kept constant for the two Delft3D models. The sediment properties applied can be found in Table 3. The first three classes "Sand" to "Very fine sand" are modelled as non-cohesive material with typical realistic values for quartz sandstone which has a specific density of approximately 2650 kg/m³ and a dry bed density of 1600 kg/m³. The two other sediment classes, "Silt" and "Clay" are modelled with a dry bed density of 500 kg/m³. Since these two fine grained classes represent the cohesive material they also have values specified for their critical shear stress for erosion, settling velocity and an erosion parameter. Apart from the physical parameters that define the behaviour of the sediments according to the hydrodynamics, various numerical parameters have to be defined which are more related to the way the program engine applied the physical basis in the numerical simulation. A summary of the additional parameters that were used for the simulation can be found in the appendix. Not all of these parameters are explained here in detail. Noteworthy to mention however is the morphological acceleration factor which is a way to speed up the computational time needed to create the simulation result by multiplying the outcome for each hydrodynamic time step by the morphological scale factor (Roelvink, 2006).

A top view of the Delft3D models at the end of the simulation is presented in Figure 10.

Table 3: Sediment physical parameters applied to the Delft3D-Flow simulations

Type of Sediment	Medium -fine sand	Fine - very fine sand	Very fine sand	Silt	Clay
D50: mean grain size	250 µm	150 µm	100 µm	17 µm	4 µm
Critical Shear Stress for erosion [N/m^2]	-	-	-	2	2
Settling velocity [m/s]	-	-	-	0.8	0.0144
Dry bed density [kg/m^3]	1600	1600	1600	500	500
Specific density [kg/m^3]	2650	2650	2650	-	-
Erosion Parameter [kg/m^2/s]	-	-	-	0.0001	0.0001
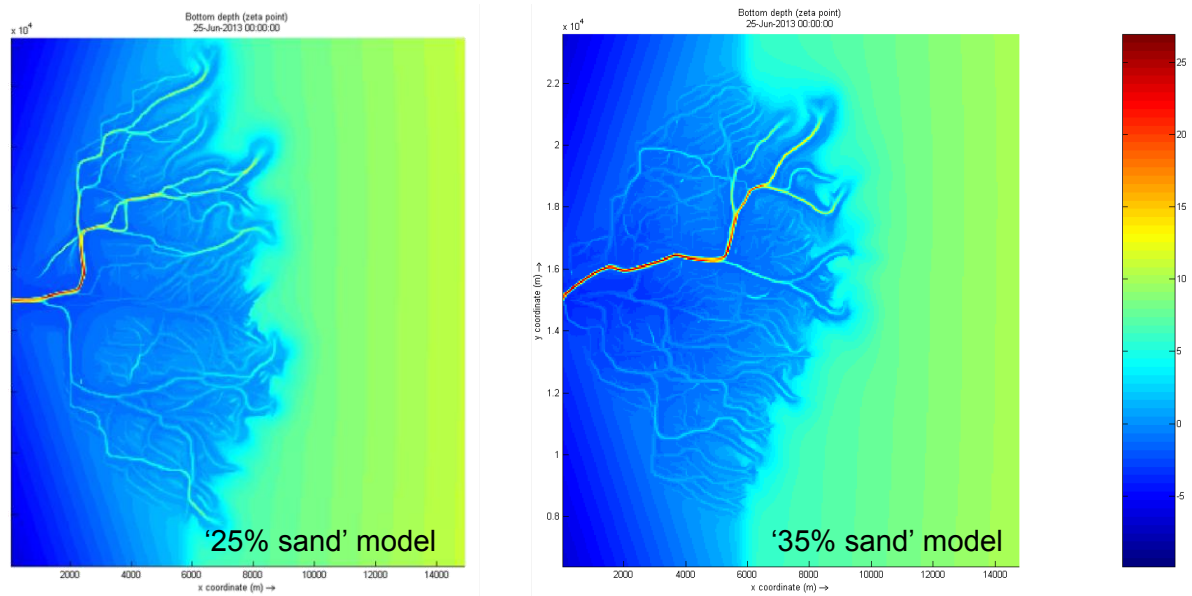
Figure 10: Top view of the final bathymetry of the created Delft3D models.

Delft3D output files

The output of a Delft3D simulation consists of one file (trim file) containing various variables. A detailed description on these can be found in the user manual (Deltares, 2011). The matrix with the grain size distribution in each grid cell is saved in the 'f_b'-variable. This 4D-matrix comprises the fraction of the mean grain size of the five grain classes (e.g. 250μm sand, 150μm sand etc.) in each cell of the finite element grid of the Delft3D model. The sum of the five grain classes equals the value 1 for each cell of the grid. The 'f_b'-file is the only output file that is used for the generation of the synthetic reservoir models of this study. In this study the topographic data which is saved in the separated 'z_b'-file is neglected (see Figure 11). For the scope of this study this simplification had to be made to proceed and to reach the outcomes in an acceptable time frame.
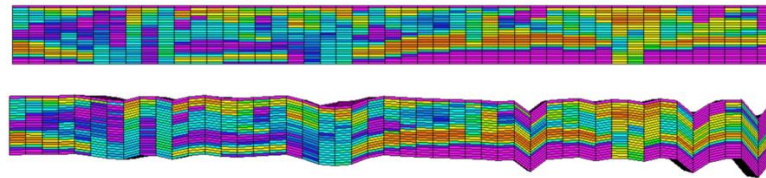
Figure 11: Cross section of Delft3D model with flattened topography (top) and the same model including topographic data (bottom), vertical exaggeration 5x

Neglecting the topographic information leads to errors of the true location of grid cells (see Figure 12). The error of vertical displacement of the model excluding the topography is between 0m and 0.3m in areas away from active channels and rises to values up to 2.5m in the vicinity of one grid block to active channels. In the channels themselves the vertical mismatch can lead to errors in the range of 10 m, in extreme cases close the river apex incisions of 22m have been observed. The errors between 0m and 1.5m represent a displacement of 0 – 5 grid cells vertical in the model which is the case in majority of the synthetic model. This is regarded acceptable for the dynamic flow simulation. The high errors in the channel centre will be addressed in the following chapter.
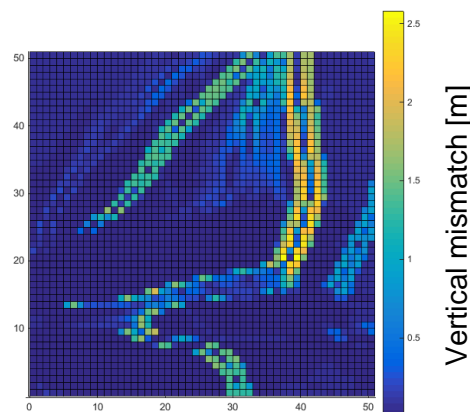
Figure 12: Errors created by neglecting topography from the 'z_b'-file from Delft3D

3.2. Modelling of the sequence stratigraphy

After having created the Delft3D delta models, the next step was to specify the sub-domain of the model that was used in the flow simulation. The target of this step is to create different stacking patterns with the Delft3D models. With Delft3D it is not possible to simulate a succession of several deltaic build-outs in one single simulation run. Therefore the stratigraphic stacking is done manually by taking sub-domains of Delft3D model which are stacked onto each other. Sub-domains of 50 x 50 grid blocks (2500 m x 2500 m) are taken from the Delft3D model. Then, successions of three 50 x 50 sub-domains (each represent an individual parasequence) are stacked onto each other in order to model the sequence stratigraphic context such as progradation or a retrogradation of the delta (see Figure 13). The sub-domain sizes of 50 x 50 grid blocks over the three parasequences result in a grid of $2.6 *10^5$ grid cells.

For the dynamic fluid flow simulation in Eclipse (SCHLUMBERGER, ECLIPSE Reference Manual Version 2013.2, Technical Description, 2013) the chosen model dimension are considered to have the best ratio between the size of the reservoir model and the time needed to execute one simulation. For this work, a script was programmed in MATLAB (The Mathworks Inc., MATLAB Version R2014b) that provides the user a tool to define which model segments should be stacked onto each other. In a prograding delta case for example, the lowermost parasequence is taken from a distal location of the Delft3D model. The subsequent parasequence that overlays the lower one then chosen from a location from an intermediate distance from the coastline. The uppermost sequence is extracted close the shoreline, respectively. In an aggradational stacking pattern, three individual parasequences are chosen which lie approximately in the same distance from the delta apex. The retrogradational stacking pattern model consists of the identical parasequences to the progradational setting but in a reversed order so that the proximal deposits get overlain by more distal deposits. By doing so, a direct comparison can be made between the effect of the stacking.
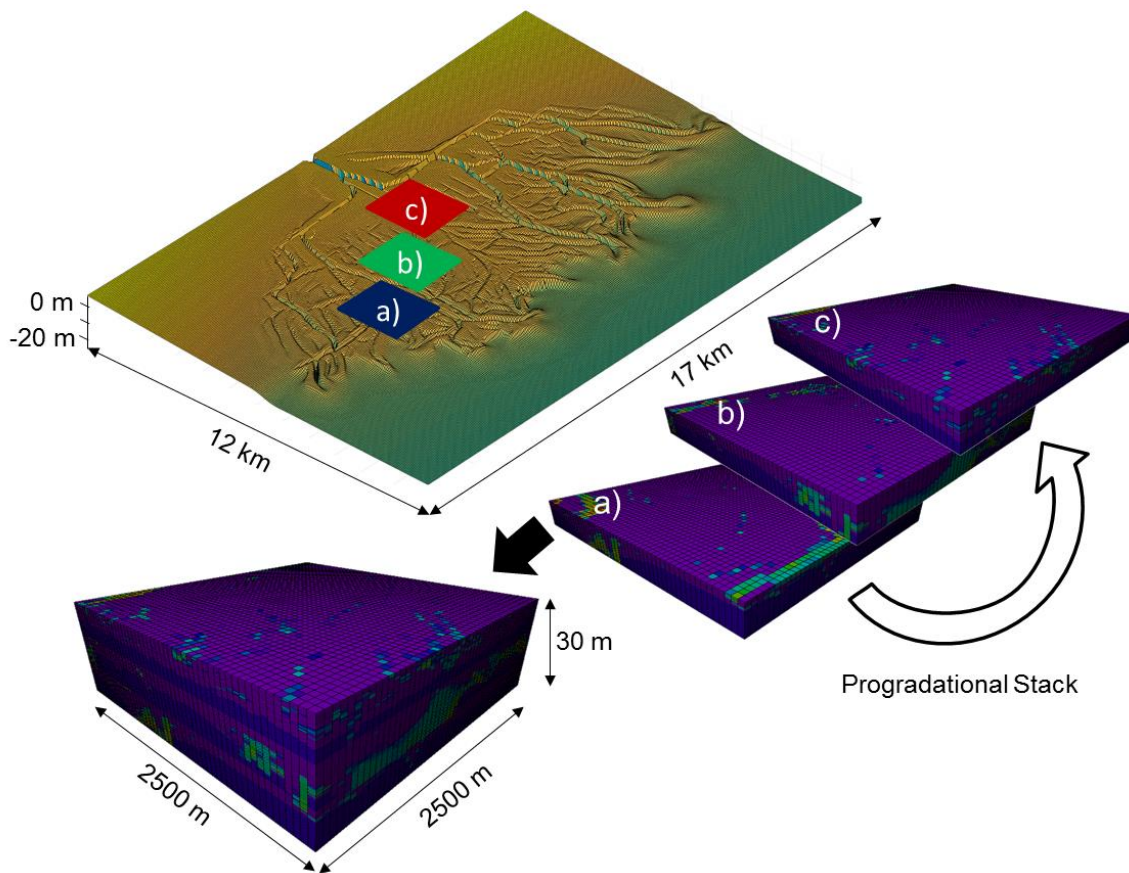
Figure 13: Example of progradational parasequence stacking

Stacking the deltaic deposits in such a way cannot be achieved by only adding up the individual parasequences because that neglects any reworking of older deposits which could potentially be incised by younger channels of the subsequent parasequence. Pure adding treats each parasequence as an isolated deposit without any interaction of what is lying above and below its interval. In order to generate more realistic reservoir architecture a solution has been developed which follows two basic rules:

1) After deposition of a sequence the top surface is covered by one grid block of shale (30 cm).
2) Active cells at the base of the sequential parasequence incises 5 grid (1.5 m) blocks into the older strata, eroding and replacing the grid cell properties of the lower deposits (see in Figure 14)

This has been implemented for the mid layer eroding into the lowest strata as well as the top sequence into the mid layer. An example of an incision is given in Figure 15.
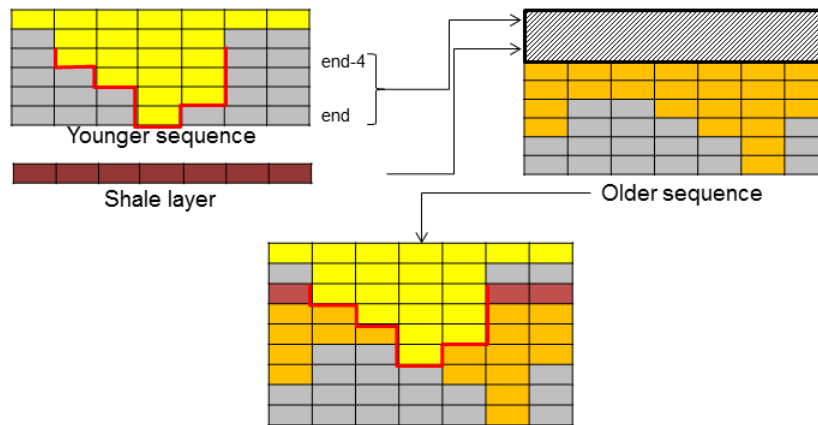
Figure 14: Schematic drawing of the stacking of individual Delft3D models in cross sectional view. Yellow and orange colored grid cells represent arbitrary cell attributes of individual parasequences
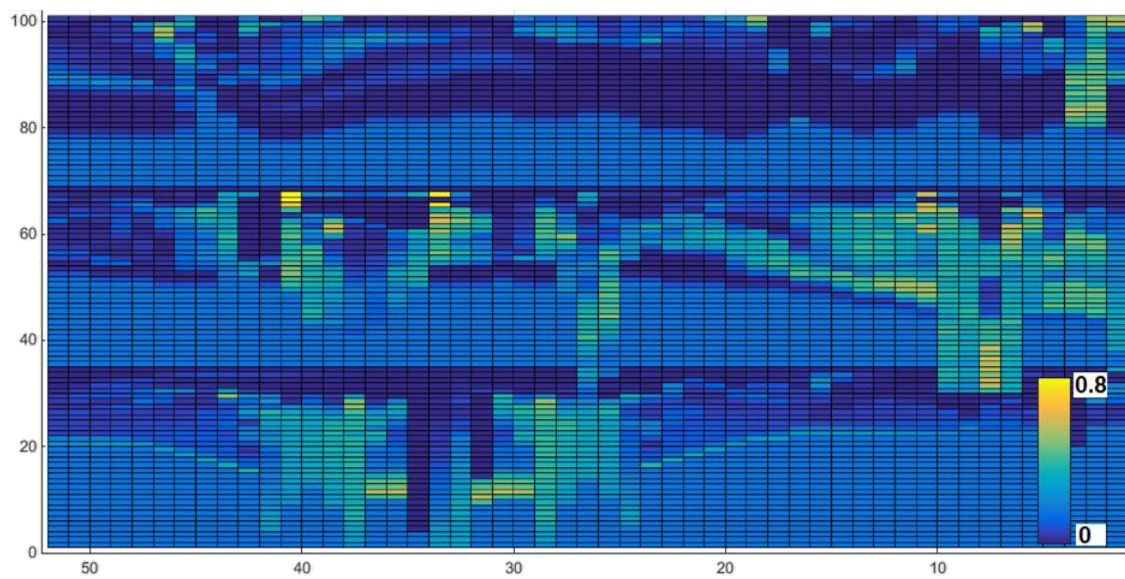
Figure 15: Example of an arbitrary cross section after stacking and incision. Property shown is the third volume fraction (D50 = 100 μm)

3.3. Implementing mechanical unit confined fractures in Petrel

Mechanical units were defined in order to divide the synthetic reservoir model into sediment packs with similar petrophysical properties. In a second step these defined mechanical units should be modified by a fracture network in order to reach a realistic reservoir model.

The grid cells with the mechanical unit representative for the coarsest grained sediments will be subsequently filled by fractures. A grid cell is assigned to the mechanical unit if the sum of the fraction of coarsest grain size (D50=250µm) and the second largest grain size fraction (D50=150µm) is larger than 80%. If these conditions are not met, the grid cell is classified as mechanically soft material which is less favourable to fracture.

The coarse grained grid cells are mainly found in vicinity of channels and close to the river apex and follow therefore often the sedimentological trend (see Figure 16). Once the mechanical units were defined, surfaces were generated which follow the base and the top of each mechanical confined layer at the base and the top. After that, zones were created from the surfaces. In Petrel it is only possible to truncate fractures by zones. Zones are volumes which are bounded by surfaces. Once this was achieved, stochastically generated fractures were truncated by these surfaces/zones.
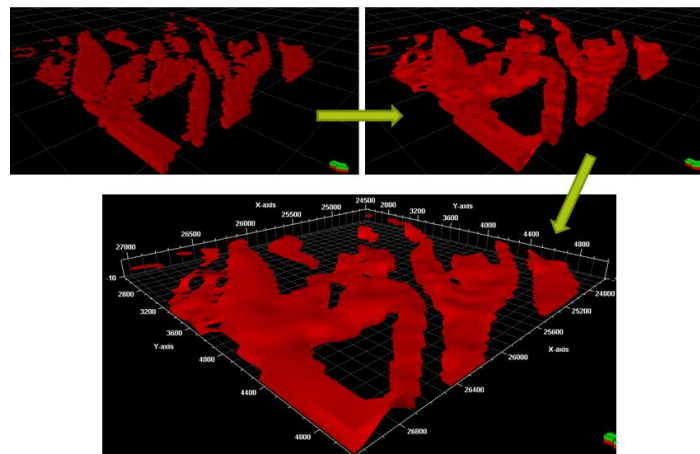
Figure 16: Workflow going from a discrete class of Mechanical Unit to surfaces. Grid cells with mechanical unit condition (top left), replaced by surfaces (top right) and final surface (bottom)

Fractures are placed within the mechanical unit based on uniform centroid placement. The placement of the fractures continues till reaching the defined density value P_{32}. A summary of the fracture properties such as their distribution and geometry can be found in Table 4. These values have been chosen in a reasonable range for fractures in a deltaic setting.

In the example given below (Figure 17), a fracture network has been created for the coarsest grained mechanical unit. The fractures are vertical with a North-South strike and a fracture density of $P_{32} = 0.005$ ($P_{32} = $ total surface area of fractures / volume of rock mass). The amount of fractures which are truncated by top and base of the surfaces is 80 %, the remaining 20 % penetrate through all the layers. By doing so, the models mimic the fracture characteristics which were observed in outcrops, namely that big fractures can cut through small shale layer and thus connect between sand bodies. However, since most of the fractures are determined to be confined to the mechanical layer, these do not impact the vertical connectivity in the reservoir (see Chapter 2.4 Origin and formation of unit confined fractures). Therefore a truncation probability of 0.8 was implemented.

Eclipse calculates flow not through discrete fractures but through the 3D grid. The upscaling of the discrete fracture network translates the discrete fracture transmissibility into a continuum grid based permeability distribution (see Figure 17). The output of the fracture generation consists of four individual properties. One contains information about the porosity and the other three for directional permeability value (vertical permeability, permeability along the fault plain and permeability perpendicular to the fault plain). Once the upscaling is done, the upscaled fracture grid cells can be added to model and the fluid flow simulation can start. Where fractures indicated the permeability of the grid cell is usually increased by 10-20 mD in the vertical as well as the direction of the fracture. Perpendicular to the fracture surface the permeability is modelled as constant. At the start and end of the fracture a value of half the middle permeability is given.

Table 4: Definition of fracture properties for the implemented fracture network in Petrel

Distribution	Extent			
		Truncated by top	80 %	
		Truncated by base	80 %	
	Distribution			
		Density definition	P_{32}	0.005
Geometry	Shape			
		Number of Sides	4	
		Elongation Ratio	2	
	Length			
		"Power" Model		
		Constant parameters	Shape: 2.1 Scale: 25 Max. 1000	
		Max. length of implicit fractures	150	
Orientation	Method			
		Fisher model		
		Constant parameter	Mean dip: 90, Mean dip azimuth: 0, Concentration: 40	
Aperture	Apertures	Log-normal, Constant parameters	Mean: 0.000075, Std. dev.: 0.0000015 Max: 0.005, Min: 0	
	Permeabilities	Correlate permebilities to apertures		
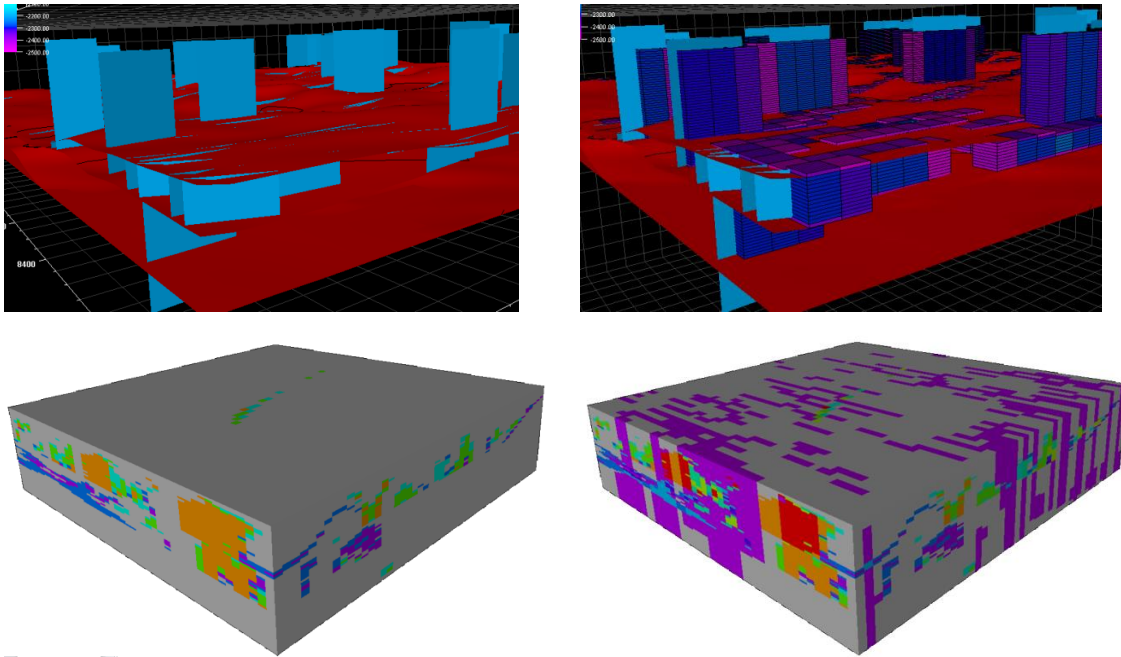
Figure 17: Mechanical unit confining surfaces in red with fractures in blue (top left), upscaled fractures (top right). Stack of three parasequences without (bottom left) and with upscaled fractures (bottom right).

3.4. Reservoir Property determination

In order to run reservoir simulation with Eclipse various reservoir property parameters have to be defined. These include properties such as: porosity, permeability, Net/Gross-ratio, saturation and reservoir pressure. For all models used in this study, the determination is generalised in such a way that all values are based on the particle-size distribution (Vol_frac).

The porosity and permeability was not calculated directly in the Delft3D models. These properties have to be derived from parameters of the grain-size distribution (Panda & Lake, 1994). The distribution of grain sizes contain various parameters which can be used for the approximation of porosity and permeability. These parameters include the mean (μ) of the distribution, the standard deviation (σ) and the skewness (γ). A plot of the grain diameter against fraction on a linear scale shows that the distances between bins are dispersed over a wide range (see Figure 18).
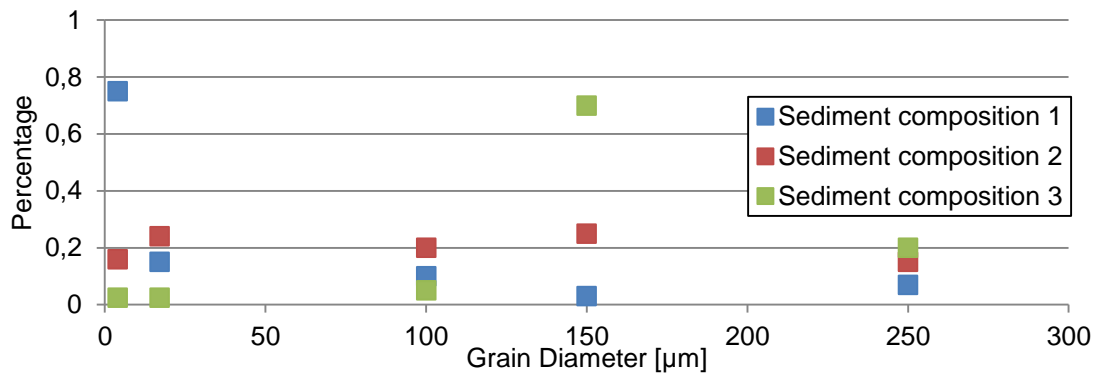
Figure 18: Example of three different sediment compositions (Sediment 1-3) expressed in the five grain size classes on a linear scale

It is straightforward to calculate the mean value for each of the three sediment compositions. However, fitting a curve through such a distribution in order to determine the statistical parameters required for the porosity/permeability calculations (such as the variance and the standard derivation) is harder. Plotting D_P on a logarithmic Krumbein-Phi-Scale which is computed by the equation

$$\Phi = -log_2 D_P$$

a distribution curve can be fit with a much higher confidence to the grain size distribution (Figure 19). The grain size distribution on a Phi-scale ranges from smaller than "-8" for boulders to larger than "8" for mud (see Table 5). Grain sizes ranging from sand to silt are situated in the window between "-1" and "8".
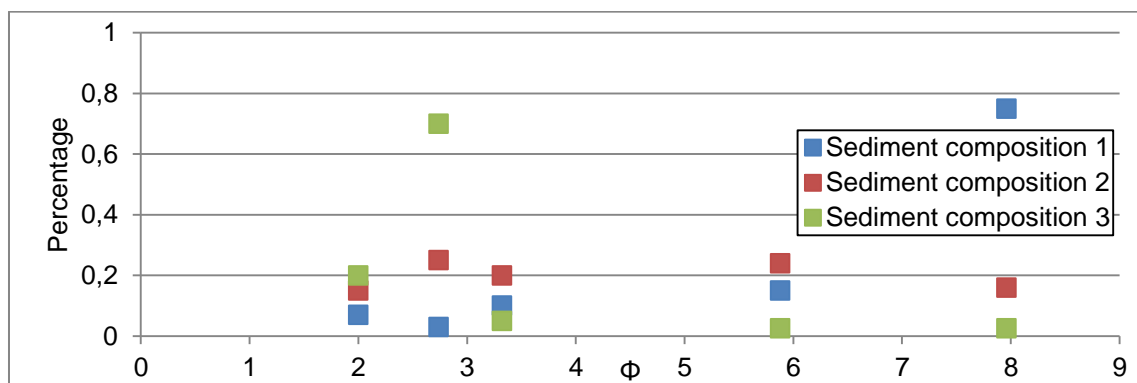
Figure 19: Sediment compositions on a Krumbein-Phi-Scale

Table 5: Conversion for grain sizes from metric to the logarithmic Krumbein-Phi-Scale

Phi scale	Metric scale	Aggregate name
>8	>256 mm	Boulder
-6 to -8	64 – 256 mm	Cobble
-1 to -6	2 – 64 mm	Pebble
1 to -1	0.5 – 2 mm	Coarse to very coarse sand
2 to 1	0.25 – 0.5 mm	Medium sand
4 to 2	62.5 – 250 µm	Very fine to fine sand
8 to 4	4 – 62.5 µm	Silt
15 to 8	<4 µm	Clay

Given the grain size distribution on a log-scale it is possible to fit a normal distribution constrained to the bin location of any given fraction distribution of the sediments from which the statistical parameters such as the mean, the standard deviation and the skewness can be determined. The density function of a log-normal grain size distribution is defined as

$$p(\Phi) = \frac{1}{\sqrt{2\pi\sigma_L}} exp\left[-\frac{(\Phi - \Phi_\mu)^2}{2\,(\sigma_L)^2}\right]$$

where σ_L is the standard deviation, Φ the normalized grain diameter and Φ_μ the geometric average of grain size.

The porosity of a given grain composition is predicted using an empirical correlation which is based on the sorting of the sediment coefficient. The sorting is obtained from the standard derivation (σ) of the grain size distribution. In the literature studies are available that deal with the correlation of standard deviation of the grain size distribution of bed material and porosity (Takebayashi & Fujita, 2014). An empirical correlation was established which was supported with field data that was obtained from fluvial deposits of the Kizu river in Japan (see Figure 20).

As can be seen in the graph, the uncertainty of porosity prediction increases with higher standard deviations. Errors of +/- 10% porosity are probable. This uncertainty is regarded to be acceptable for this study. A fitting curve is extrapolated through the given field data points and used for the porosity calculation of the Delft3D models. The empirical fit is given by the formula

$$Porosity = C_1 * \frac{C_2\ \sigma^{C_3}}{1 + C_2\ \sigma^{C_3}}$$

where C_1 = 0.38, C_2 = 3.7632 and C_3 = -0.7552

An expression for the correlation of particle size distribution with permeability is provided in the literature (Panda & Lake, 1994). Estimating permeability includes more parameters and is somewhat more complex compared to the porosity prediction. The correlation is based on the basic Carman-Kozeny method where the permeability is derived from fluid conservation equation on a microscopic scale and upscaled and extrapolated to the ratio of flow rate against the pressure gradient at a local scale. In an ideal case of perfectly rounded grains with a diameter D_P, tortuosity τ the permeability k becomes:

$$k = \frac{Dp^2\ \varphi^3}{72\tau(1 - \varphi)^2}$$

Panda and Lake altered this formula so that the permeability k can be calculated from parameters from the particle size distribution. The formula changes to the form

$$k = \frac{Dp^2\ \varphi^3}{72\tau(1 - \varphi)^2}\left[\frac{\left(\gamma C_{Dp} + 3\ C_{Dp}^2 + 1\right)^2}{\left(1 + C_{Dp}^2\right)^2}\right]$$

where C_{Dp} is the coefficient of variation of the particle size distribution (σ/D_p).

A MATLAB function is implemented in order to populate the entire delta model with the properties porosity and permeability (see Figure 21).
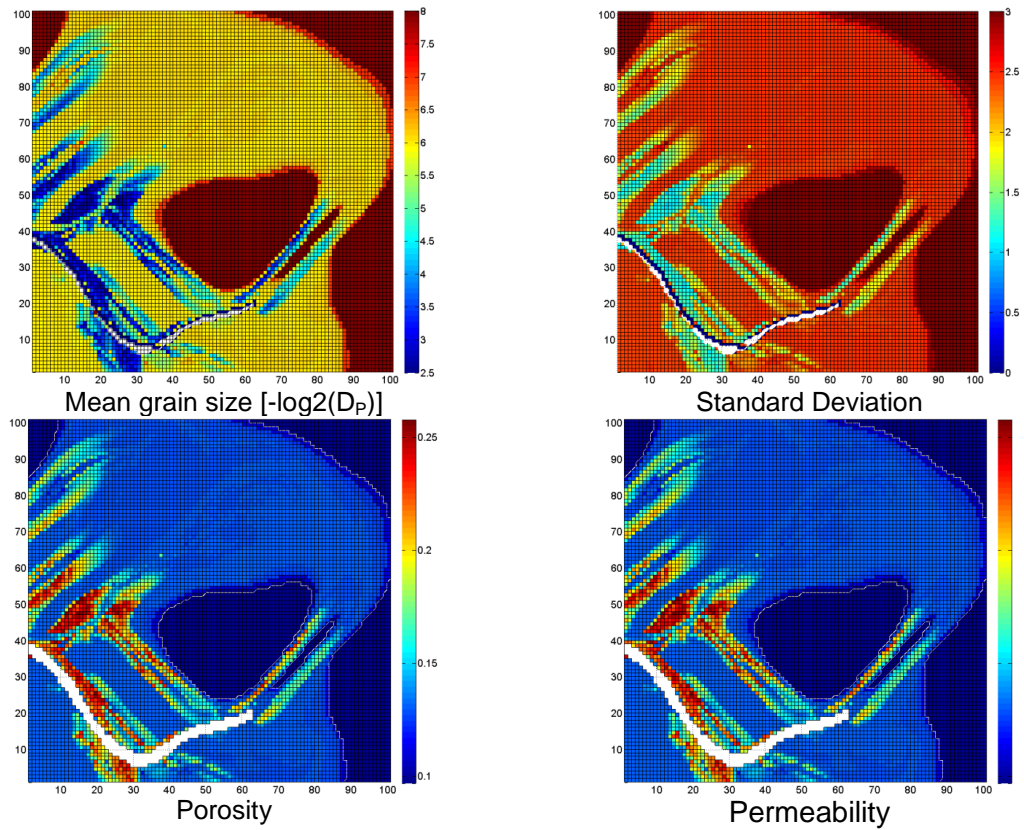
Figure 21: Example of a Delft3D grid from top view. Mean grain size (top left), standard deviation (top right) from which reservoir properties porosity (bottom left) and permeability (bottom right) are derived

3.5. Reservoir Conditions

Furthermore, flow simulations require assumptions on the property of the reservoir liquids and the rock-fluid-physics. The standard black oil model for the oil and water phases was selected (see Table 6). The rock physics function takes oil and water into account and neglects gas. The relative permeability and capillary pressure curve used for the simulation are given below (see Figure 22). The relative permeability curves define a conate water saturation of S_{wc}=20% and a residual oil saturation of S_{or}=25%. Therefore the initial oil saturation at the beginning of the simulation (S_O (t=0)) is modelled as

$$S_O(t = 0) = 1 - S_{wc} = 0.8$$

The movable oil volume MOV is hence calculated as

$$MOV = 1 - S_{wc} - S_{or} = 0.55$$

The values are obtained from the Corey correlation. The correlation is applicable for slightly consolidated sandstones. For the compaction of the rock the pre-defined Petrel model for "Consolidated sandstone" is chosen. The reservoir conditions were kept constant for the entire study. The differential between reservoir pressure and bubble point pressure is set to high values in order to suppress any interactions with a gas phase in the simulations in Eclipse.

Table 6: Reservoir conditions and properties of reservoir fluids

Reservoir	Min. pressure: 60 bar	Max. pressure 250 bar
Conditions	Temperature: 90 C˚	Reference Pressure: 200 bar
Oil Property	Density: 854 kg/m^3	Bubble point: 30 bar
Water Property	Salinity: 18000 ppm	
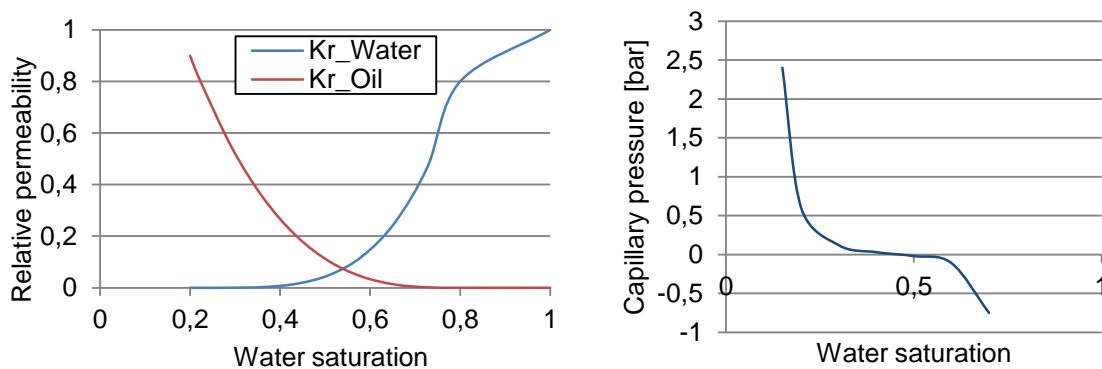
Figure 22: Oil and water relative permeability relationship (left) and capillary pressure curve (right)

3.6. Well spacing strategy

A total number of 12 well locations are defined for each reservoir model, of which 6 are production and 6 are injection wells. One simulation always consists of one injector-producer pair such that 6 simulations are defined in total for each reservoir model. The well pairs 1-3 are orientated in a stream-wise direction and well pairs 4-6 are orientated in a span-wise direction to the fluvial inlet. The wells are located at the boundaries of the reservoir model (see Figure 23). Therefore the distance between all injection and production wells are constant at 2.5km. All the water injection wells are controlled by a bottom hole pressure of 230 bar and production wells are controlled by a bottom hole pressure of 150 bar. In order to create functioning wells in Petrel a completion of the wells was modelled. The completion consists of a casing, tubing with a packer and perforation of the casing at the reservoir interval.
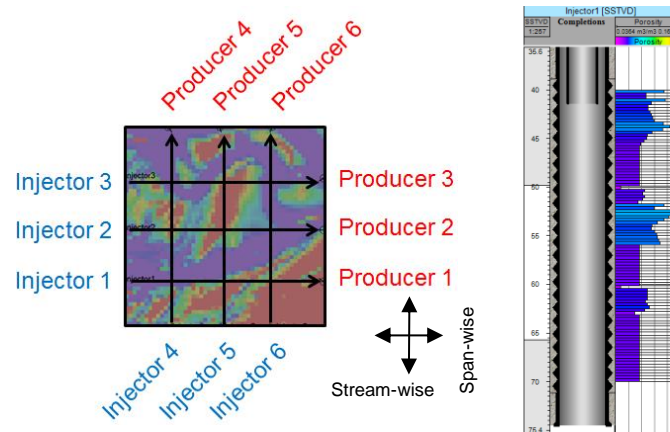
Figure 23: Well pairs used for the simulation (left) with well completion (right)

3.7. Approach for the data analysis

The dynamic simulation results that were created for this study were approached in three ways: (1) Flow response analysis (2) Analysis of average permeability maps (3) Sweep efficiency of individual parasequences. Subsequently, the results of all the simulations are compared.

Flow response analysis

The production rates over time of the oil and water phase were investigated for all 8 synthetic geological models (see Figure 24 for example). These rates provide an insight in the potential production behaviour and the life expectation of a reservoir unit as it might be obtained from a well in reality. The production result for each of the 8 synthetic reservoir model was plotted on two different graphs, one for well pairs which are orientated stream-wise (well pairs 1 – 3) and one for those that are orientated span-wise (well pair 4 – 6). Each simulation result

Figure 24: Example of the production rates over time for three wells with stream-wise well orientation

consists of two graphs, one for the oil production rate (QO) and one for the water production rate (QW).

Analysis of average permeability maps

The production data obtained from the *Flow response analysis* was subsequently compared to permeability maps of the related synthetic geological model. These maps show the average permeability of each parasequence of the synthetic reservoir model (see Figure 25). On these maps it is indicated (in black) where the layers are incised by the overlying layer. The results provide a link between the flow rate response and the characteristics of the permeability distribution within each parasequence of the synthetic reservoir model.
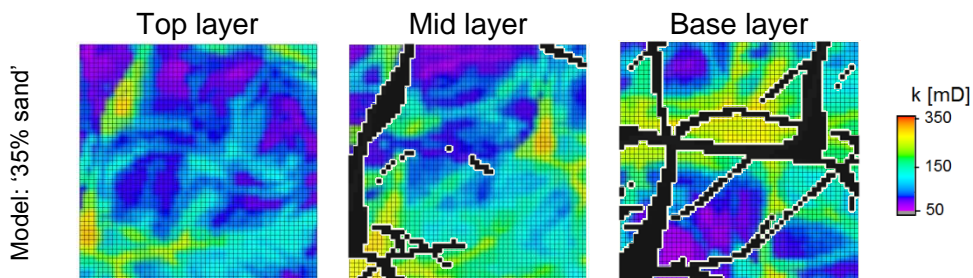
Figure 25: Example of layer averaged permeability maps with incisions

40

Sweep of individual parasequences

The third analysis which was used to characterise the flow behaviour is the sweep efficiency through the individual parasequences (see Figure 26). The sweep efficiencies are calculated as the volume of oil extracted by the end of the simulation (t = 50 years) over the initial movable oil volume (MOV) of the parasequence. As an example, a sweep efficiency of 50% for a parasequence means half of the movable oil is extracted. With the additional data it is possible to quantify the contribution of each of the three parasequences during the flow simulation. The sweep efficiencies of the

Figure 26: Example of sweep efficiency per layer

individual layer are linked to both the flow response analysis as well as the average permeability maps for each parasequences.

Model comparison analysis

The time of water breakthrough is plotted against peak production oil flow rate of all the models. The plot gives indications on how quick the injection fluid reaches the production well and how good the connection is between the injector and producer expressed by high peak oil production rates. Additionally, the pore volume injection required for a water cut of 50 % to be reached is plotted against the cumulative oil production. This parameter gives further indications how efficient the injection is in terms of oil.

41

4. Results

First the results from the synthetic reservoir models with an aggradational stacking pattern are presented (see Figure 27). The results of the '25% sand' model are presented and subsequently the results of the '35% sand' model. For each of the two models, first the results with a well orientation in a stream-wise direction are given and after that the results from a well orientation in a span-wise direction. The results are presented according to the three analysis methods that are explained in the previous chapter. After all results are presented for the aggradational stacking pattern, the results from the retrogradational and progradational stacking pattern are presented. Then the model comparison analysis follows. Finally, the results from the synthetic reservoir models with mechanical unit-confined fractures with different orientations are presented.

Delft 3D Model	Stacking pattern	Well orientation with respect to coastline		Simulation No.
D3D model: '25% sand'	Aggradational	Stream-wise	Span-wise	1 2 3 4 5 6
	Retrogradational	Stream-wise	Span-wise	7 8 9 10 11 12
	Progradational	Stream-wise	Span-wise	13 14 15 16 17 18
D3D model: '35% sand'	Aggradational	…		19 20 21 22 23 24
	Retrogradational	…		25 26 27 28 29 30
	Progradational	…		31 32 33 34 35 36
Fracture Study				
D3D model: '25% sand' Stacking pattern: 'Retrogradational'	Fractures Stream-wise	…		37 38 39 40 41 42
	Fractures Span-wise	…		43 44 45 46 47 48

Figure 27: Simulation overview with the first set of aggradational simulation (in red boxes)

4.1. Simulation results from aggradational stacking

Flow response analysis

Figure 28 shows the production curves over time for models with aggradational stacking for the oil and water phase. In total 12 model results are displayed. The results for the '25% sand' model in the aggradational stacking are shown in Figure 28 (A) & (B). The graph of (A) shows the production rates for well pairs that are orientated in the stream-wise direction and

(B) the well pairs which are orientated parallel to the coastline. The graphs in Figure 28 (C) and (D) show results for the '35% sand' model with aggradational stacking with well pairs in a stream-wise and in a span-wise direction.

The production rate for the '25% sand' model with an aggradational stacking pattern reaches their peak after 30 years and then declines towards the end of the simulation while simultaneously the water production rate inclines. The production plateau varies between 140 and 150 m^3/day with a mean of 145 m^3/day. The step-like shape of the declining curve after the first water breakthrough shows the arrival of injection water in each of the parasequences and consequently a rapid decline of oil production for that particular parasequence. Approximately by the end of the simulation, the water production rate crosses the oil production rate meaning that a water cut of 50% is reached.

The production with span-wise well pattern in the '25% sand' reaches a peak production between 125 and 150 m^3/day and a timing of the water breakthrough between 30 years (for the high peak producer) and 32 years (for the low peak producer). Compared to the well pairs which are orientated in a stream-wise direction, the span-wise well production curves show a higher variance in the peak production rate of oil, although lower production rates lead to longer time to water breakthrough.

The production with a stream-wise well pattern in the '35% sand' model also shows a water breakthrough after approximately 30 years for two of the three simulations (see Figure 28 C). The mean of the peak production is 170 m^3/day including the extreme outlier well pair 2 and 160 m^3/day excluding the well pair 2. The well pair 2 of this model shows a peak production of 225 m^3/day at an early water breakthrough after 23 years. In that case a water cut of 50% is already reached after 40 years.

The production in a span-wise direction of the '35% sand' model results in a peak production rate between 130 and 170 m^3/day with a timing of water breakthrough between 30 and 31 years. Compared to the results of the span-wise wells of the '25% sand' model, the declining curves of the oil rates after water-breakthrough in the span-wise '35% sand' model of well doublet 4 and 5 do not show an intermediate plateau close to the end of the simulation.

Flow response analysis of aggradational stacking pattern. A) '25% sand' model, stream-wise wells B) '25% sand' model, span-wise wells C) '35% sand' model, stream-wise wells D) '35% sand' model, span-wise

Figure 28: Flow response analysis of aggradational stacking pattern. A) '25% sand' model, stream-wise wells B) '25% sand' model, span-wise wells C) '35% sand' model, stream-wise wells D) '35% sand' model, span-wise wells

Analysis of average permeability maps

The production data itself is insufficient to explain outliers such as the production curves of the '35% sand' model (Figure 28 C). Further insights into the flow behaviour can be gained from the maps of vertically averaged permeabilities per parasequence (see Figure 29). These maps indicate the distribution of high permeable areas within each of the parasequences. Moreover, they show where a parasequence is incised by the overlying layer. Where an incision occurs, the vertical reservoir connectivity is usually increased.

The average permeability maps of the '25% sand' show increased permeability zones (indicated by bluish to yellowish colours) in the upper part of the base layer and in the bottom part of the mid layer. The permeability is approximately 150mD, locally it reaches 200mD. The base layer shows the trend of high permeable areas with an orientation from top-left to bottom-right and the mid layer an orientation of high permeable zones from bottom-left to top-right. From the lower left to the upper right corner an incision from the mid layer into base layer leads to vertical connection of these two layers. The top layer has less permeable zones with an orientation from left to right and only incises in isolated spots into the mid layer.

The average permeability maps of the '35% sand' model show higher values of permeability over the three parasequences than the '25% sand' model. The base and mid layer have high permeability zones over the entire reservoir-domain with values of varying between 150-

220mD. The incision from the mid layer to the base layer covers a larger area compared to the '25% sand' model which leads to a high vertical connectivity of these two layers. The top layer has less permeable zones than the mid and base layer. Also the incision from top into mid layer is localized to a spot in the bottom-right and two isolated patches.

Figure 29: Parasequence-averaged permeabilites for the aggradational models. Black grid blocks symbolize areas of incision of the overlying layer

Sweep of individual parasequences

The dynamic results are used to calculate the sweep efficiency per layer at the end of the simulation. The results of the layer recovery factors vary between the '25% sand' model and the '35% sand' model (see Figure 30).

The '25% sand' model with a stream-wise well orientation shows the lowest discrepancy between the sweep efficiency of individual parasequences compared to the other results of the aggradational synthetic models. The difference between the sweep efficiency of the base layer compared to the mid and top layer is approximately 5% for all three well doublets. The base layer reaches sweep efficiencies of 28-30% and mid layer 24-26% and the base layer 22-26%.

The '25% sand' model with span-wise wells shows a decreased sweep efficiency for all three parasequences compared to the stream-wise well pairs. The base layer is decreased to the values 26-29%, the mid layer decreased to sweep efficiencies of 22-23% and the base layer to values of 18-20%. The mid and top layer sweep efficiencies are stronger decreased than the base layer which leads to a higher discrepancy between the sweep efficiency of the individual layers.

In the '35% sand' model with a stream-wise direction the sweep efficiencies for the base layer results 28-35%. The values are higher in comparison with the '25% sand' model with a stream-wise well pattern. The sweep efficiencies for the mid and base layer are close to each other with no more than 1% difference and the value are 20-29%. Where the sweep efficiency reaches 35% for the base layer, the sweep efficiency for the mid and top layer are also on the high side with 29% (see well doublet 2). In the other two simulations the mid and top layer reach 20%, which is lower than the sweep efficiencies for the mid and top layer in the '25% sand' model with a stream-wise well pattern.

The results of the span-wise well orientation for the '35% sand' model show base layer sweep efficiencies of 26-31%, the mid layer between 20-20% and the top layer between 16-20%. The sweep efficiencies of the simulation show the highest discrepancy between the base layer and the mid and top layer among all simulation results with the aggradational stacking. The difference is 8-10%.

Figure 30: Sweep efficiency for each of the three parasequences in the aggradational setting at the end of the simulation (t = 50 years)

4.2. Simulation results from retrogradational stacking

Flow response analysis

Figure 31 shows the production curves over time for models with retrogradational stacking for the oil and water phase. In total 12 model results are displayed. The results for the '25% sand' model in the retrogradational stacking are shown in Figure 31 (A) & (B). The graph of (A) shows the production rates for well pairs that are orientated in the stream-wise direction and (B) the well pairs which are orientated parallel to the coastline. The graphs in Figure 31 (C) and (D) show results for the '35% sand' model with retrogradational stacking with well pairs in a stream-wise and in a span-wise direction respectively.

The '25% sand' model show in the well pairs which are oriented in a stream-wise direction a peak production of 135 – 160 m^3/day (average = 145 m^3/day). The same averaged peak production rate was reached in the '25% sand' model with aggradational stacking pattern. However, the time of water breakthrough varies from 23 to 29 years among the three related well pairs 1 – 3. In aggradational stacking the breakthrough of the water at the producer was determined to be closer to time of 30 years. The decline of the oil production after water breakthrough reach an intermediate plateau after 3-4 years and then decreases sharply towards the end of the simulation.

The '25% sand' model with a span-wise well orientation (well pair 4 – 6) has a plateau oil production rate which varies between 110 – 150 m^3/day (average = 130 m3/day). For the well pair with the high plateau rate of 150 m^3/day, the water breakthrough is reached after 30 years, for the well pairs with a low production, the water breakthrough is reached after 43 years. Compared to the '25% sand' model with a stream-wise well orientation, the well pairs of a span-wise direction show less similarities among the three well pairs in terms of peak oil production rate and timing of water breakthrough.

The stream-wise wells in the retrogradational '35% sand' model are producing at a plateau rate ranging from 210 – 260 m^3/day (average = 235 m^3/day). Together with the progradational '35% sand' model, these values are the highest reached in this study with the flow simulations. The first water break-through in this model is reached between 22 – 25 years. The oil production decreases sharply and flattens out towards a second plateau which is located around 16 years after first water breakthrough (see Figure 31 C, QO2 & QO3). Simultaneously, the water production rate increases semi-linearly to the end of the simulation.

The span-wise direction of the '35% sand' retrogradational model has a plateau production varying between 165 – 180 m^3/day (average = 170 m^3/day). The first water-breakthrough of three well pairs occurs after 30 - 32 years. Like in the span-wise well orientation in the aggradational setting of the '35% sand' model, the production curves show little variances among the three related well pairs. The production rate is around 30% lower than in a stream-wise direction.
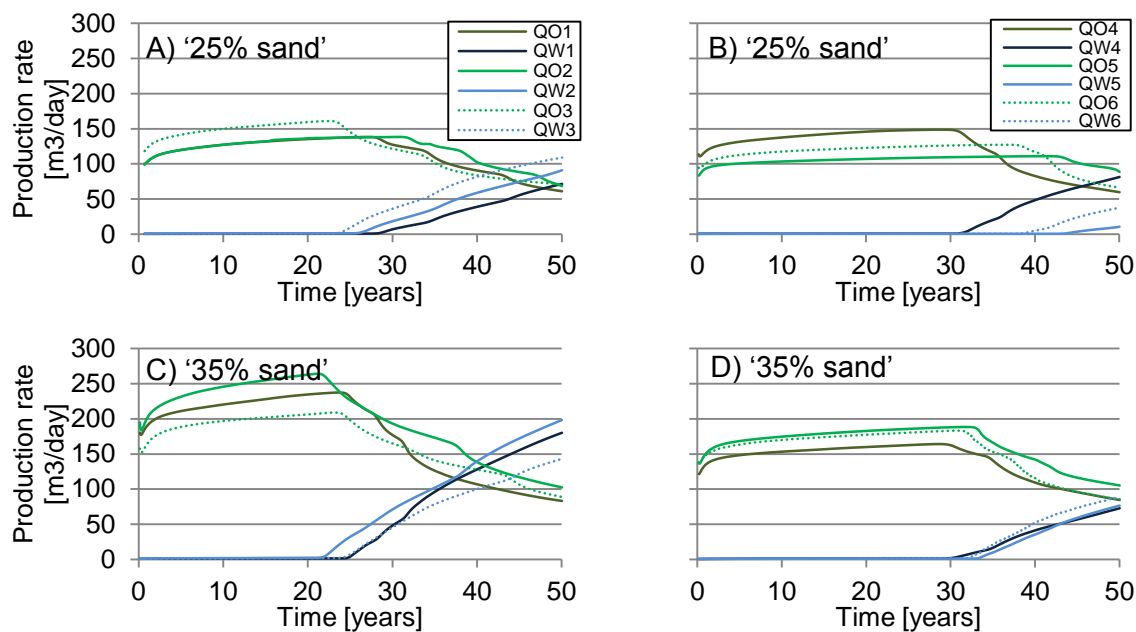
Figure 31: Flow response analysis of retrogradational stacking pattern. A) '25% sand' model, stream-wise wells B) '25% sand' model, span-wise wells C) '35% sand' model, stream-wise wells D) '35% sand' model, span-wise
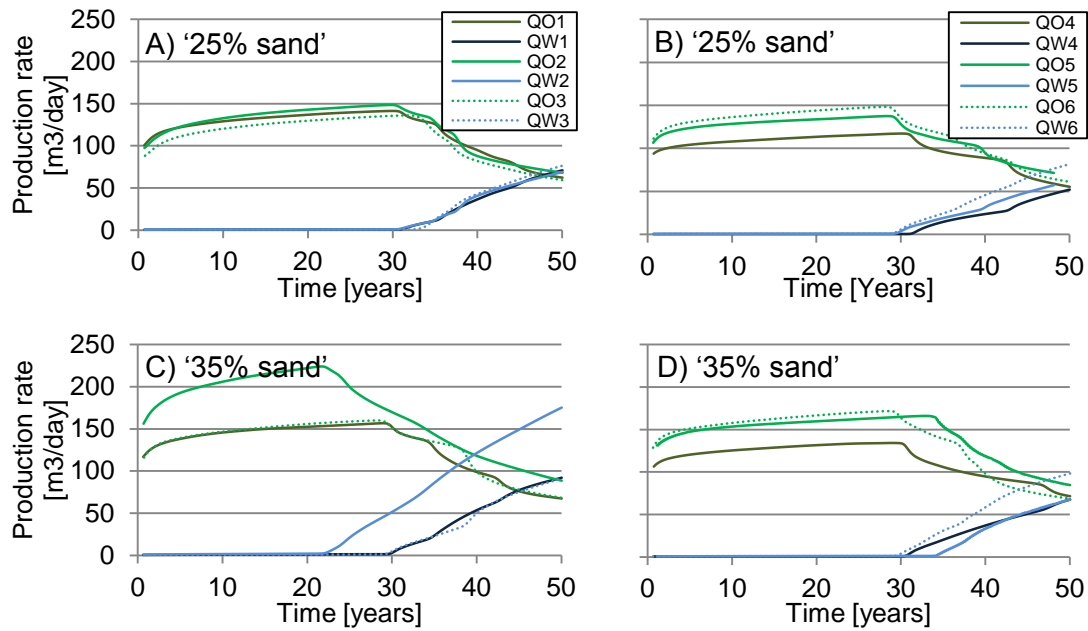
Analysis of average permeability maps

To understand the flow characteristics of each of the synthetic reservoir models with the different well orientations it is insightful to consider the vertically-averaged permeabilities for each of the layer (see Figure 32). In both the '25% sand' model as well as the '35% sand' model the permeability decreases from the base layer going upwards in stratigraphy. The base layer is taken from a proximal location close to the delta apex. It is subsequently overlain by more distal deltaic deposits. In the '35% sand' model larger areas show permeability values of 150mD or higher. In the '25% sand' model the permeable zones are more defined to elongated bodies which are bounded by the sides of low permeable substrate with a permeability of <70mD. These elongated permeable zones are present in the top and mid layer of the '25% sand' model. The base layer in both the '25% sand' as well as the '35% sand' show a left to right trending permeable zone with a width of 500 – 700m on the left boundary and a width of >2000m at the right boundary of the model. The permeability is in the range of 100-200 mD in the '25% sand' model and 150-250 mD in the '35% sand model.

The incision is higher in the '35% sand' model compared to the '25% sand' model. In the base layer of the '35% sand' model the incision from the mid layer covers big parts of the surface. The incision from top layer to mid layer in the '35% sand' model is concentrated to the left part of the model and an isolated location at the top right corner. Incision in the base layer of the '25% sand' model is defined to limited elongated areas with a diagonal

48

orientation at the lower part of the model. The incision from top to mid layer is along one elongated zone with a vertical orientation.
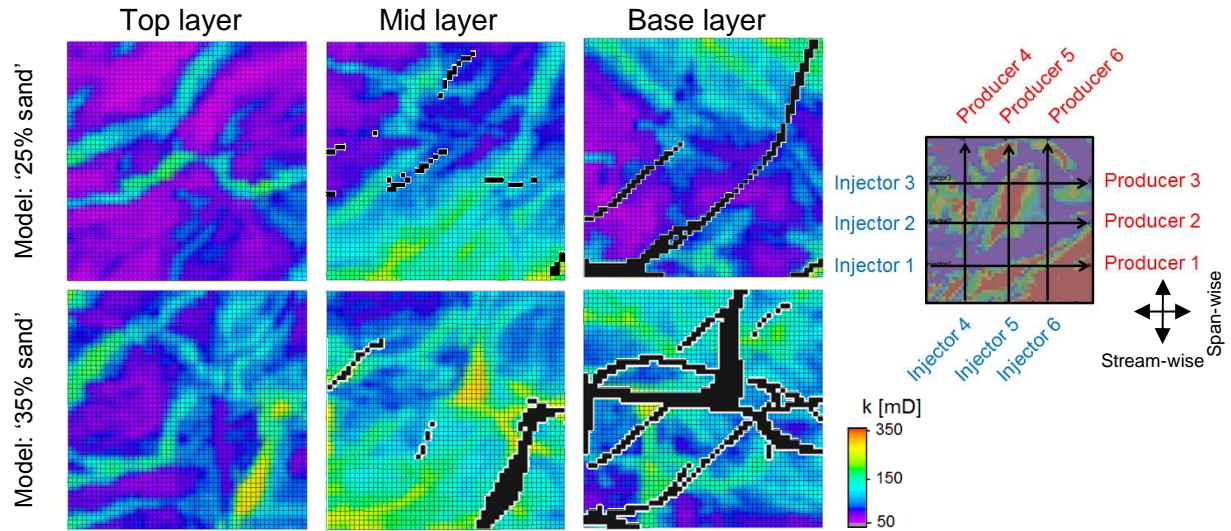

Figure 32: Parasequence-averaged permeabilities for the retrogradational model. Black grid blocks symbolize areas of incision of the above-lying layer

Sweep of individual parasequences

As in the aggradational case, the highest sweep efficiency at the end of the simulation is achieved in base layer (see Figure 33). The '25% sand' stream-wise well orientation shows the same distribution as observed in the aggradational setting, with a base layer sweep efficiency of 25-30%, mid layer sweep efficiency between 22-25% and a base layer sweep efficiency between 20-22%.

In the span-wise '25% sand' setting the sweep efficiencies for all the parasequences are close to each other varying between 20-25%. The base layer sweep efficiency is not increased as in the stream-wise direction but is similar compared to the mid and top parasequences. The well doublet 4 shows that the sweep efficiency of the top and base layer are 25% and the mid layer is 20%. No other simulation that was run in this study showed this distribution of sweep efficiencies with top and base higher of the same value and the mid layer decreased by 5%.

In the stream-wise '35% sand' model the sweep efficiency is between 23-35% for the base layer, 22-26% for the mid layer and 19-21% for the top layer. The well doublet number 2 shows the highest difference measured in this study between two sweep efficiencies of parasequences, namely from base to top layer with a difference of 14%. In contrast to that, the adjacent well doublet 1 has almost equal sweep efficiencies for all three parasequences.

In the span-wise '35% sand' model the sweep efficiency is between 25-30% for the base layer and between 16-20% for both the mid layer as well as the top layer. The difference

49

between the base layer and the other two is between 8-10%. The sweep efficiencies compared to the span-wise wells of the '25% sand' model show that the mid and top layer are both swept with a efficiency of 20% in two simulation runs (well pair 5 and 6). However, the base layer is 10% higher for the '35 sand' model.
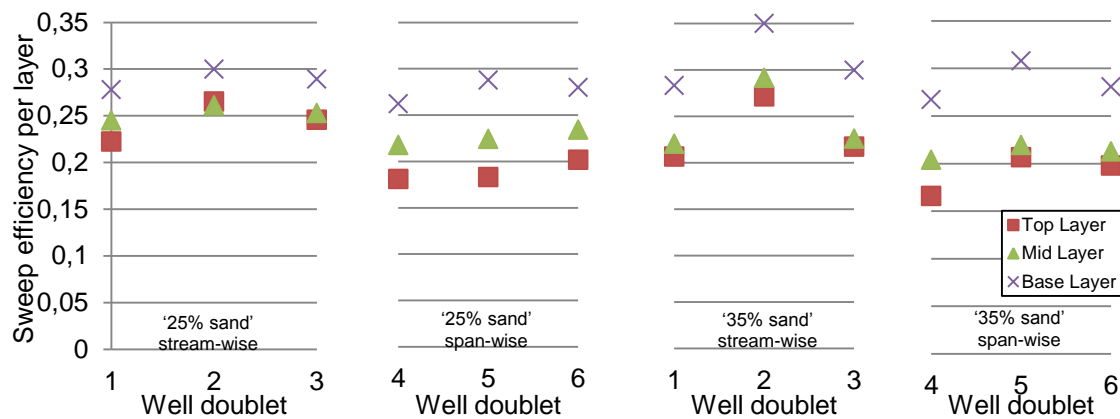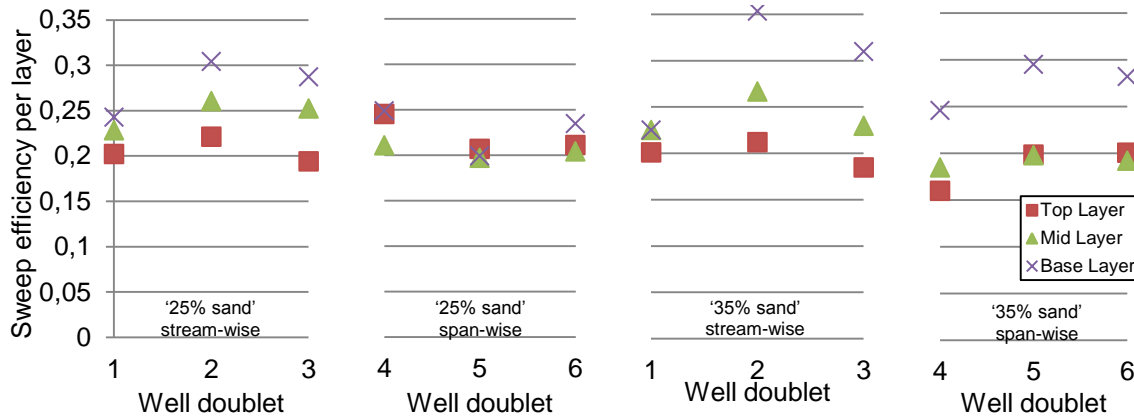

Figure 33: Sweep efficiency for each of the three parasequences in the retrogradational setting at the end of the simulation (t=50 years)

4.3. Simulation results from progradational stacking

Flow response analysis

Figure 34 shows the production curves over time for models with progradational stacking for the oil and water phase. In total 12 model results are displayed. The results for the '25% sand' model in the progradational stacking are shown in Figure 34 (A) & (B). The graph of (A) shows the production rates for well pairs that are orientated in the stream-wise direction and (B) the well pairs which are orientated parallel to the coastline. The graphs in Figure 34 (C) and (D) show results for the '35% sand' model with progradational stacking with well pairs in a stream-wise and in a span-wise direction.

In the '25% sand delta' model with a progradational stacking pattern the plateau oil production varies between 140 - 180 m^3/day (average 170 m3/day). The first breakthrough of injection water occurs between 25 – 32 years. A water-cut of 50% is reached after 41 – 49 years. The oil production declines sharply with the start of water production and flattens out towards the end of the simulation.

The span-wise well orientation for the progradational '25% sand' model results in a production plateau rate of 115 – 144 m^3/day (average: 130 m^3/day). The plateau production rate in a span-wise direction is 75% of the rate achieved with a stream-wise well orientation. The time of initial water breakthrough varies from 25 – 37 years. The production decline after water breakthrough shows an intermediate plateau leading to a step-wise decrease of the oil

50

production (see Figure 34 B, QO4, QO5 & QO6). Compared to the stream-wise wells, the decline after water-breakthrough is shallower in the span-wise orientation.

The progradational stacking pattern in the '35% sand' model reaches high oil plateau production rates in a stream-wise well orientation of 215 – 270 m^3/day (average: 240 m^3/day). The initial water breakthrough is reached after 24 – 26 years. In all three well doublet simulations a water-cut of 50% is reached between 38 – 41 years. The decline curves do not show a clearly defined intermediate plateau.

The '35% sand' span-wise well pattern results in plateau rates of 160 – 190 m^3/day (average: 180 m^3/day) which is 75% of the plateau oil production rate reached with the stream-wise well orientation. The initial water-breakthrough is reached after 31 – 34 years. The declining rates after water-breakthrough show an intermediate plateau for two of the wells (see Figure 34 D, QO4 & QO5).
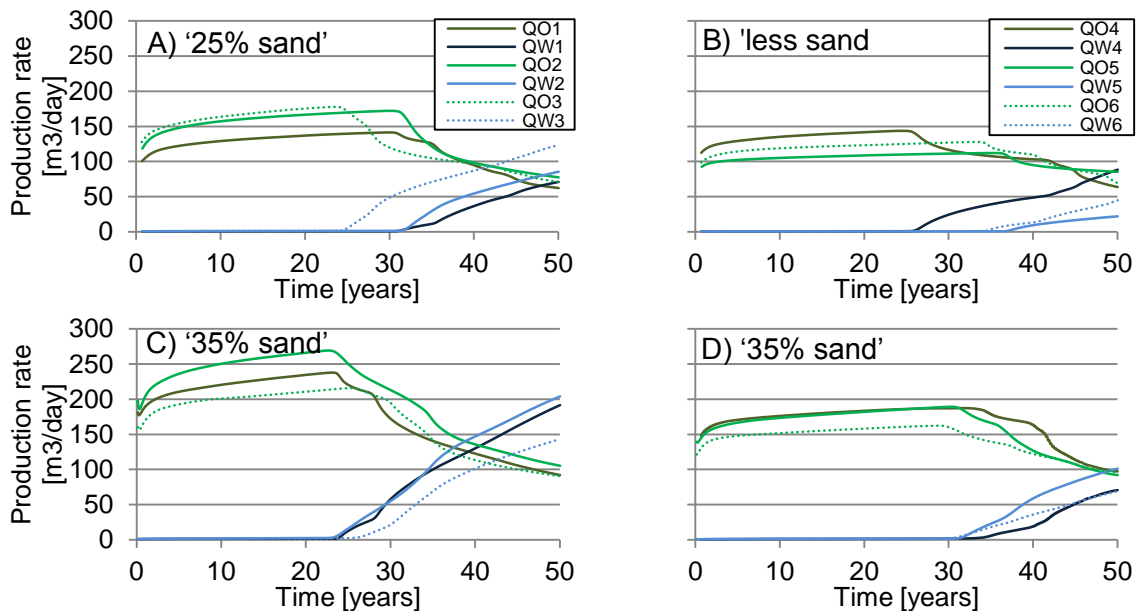
Figure 34: Flow response analysis of progradational stacking pattern. A) '25% sand' model, stream-wise wells B) '25% sand' model, span-wise wells C) '35% sand' model, stream-wise wells D) '35% sand' model, span-wise

Analysis of average permeability maps

The permeability maps relate the production behaviour with the synthetic reservoir models of the progradational stacking (see Figure 35). The individual parasequences used for the progradational stacking pattern are the same as the ones which were used for the retrogradational stacking. The order of base and top layer is changed to reach a synthetic model of a progradational setting.

In both the '25% sand' model as well as the '35% sand' model the top layer consists of a layer with a high permeability confined to a limited zone with an orientation from left to right

on the top view on the model. On the left side of the reservoir model the permeable zone has a width of 500-700m and it becomes wider going towards the right of the model to a value of >2000m. The permeability values range from 100-200 mD in the '25% sand' model and150-250 mD in the '35% sand' model.

The mid layer in the '25% sand' model has a zone of higher permeability values (100-150 mD) at the lower side of the model and rather isolated permeable zones in the upper part. The mid layer in the '35% sand' model has more highly permeable areas in the parasequence and also higher permeability values of 150-250 mD. Also here, the upper part of the model has lower permeability values as it was noted in the '25% sand' model.

The base layer for the '25% sand' model consists of isolated elongated permeable zones with a vertical to diagonal orientation and permeability values of 100-150 mD. The permeable zones are focussed in on the lower left corner on top view. The upper right corner the permeability is low <75 mD. In the '35% sand' model the permeable zone is also focused around the lower left corner with elongated permeable zones which are orientated in a vertical to diagonal orientation. The permeable zones are wider and have higher permeabilites (150 – 250 mD) compared to the '25% sand' model.

As well as in the aggradational and retrogradational reservoir models, more incision occurs in the '35% sand' model compared to the '25% sand' model. In the base layer of the '35% sand' model the incision from the mid layer covers big parts of the surface. The incision from top layer to mid layer in the '35% sand' model shows high incision in the central part of the parasequence going from the left boundary towards the right with a width of 500-700 m. Various branches of incision cover the mode. Incision in the base layer of the '25% sand' model is defined to limited elongated areas with a diagonal orientation at the lower part of the model. The incision from top to mid layer is predominated by a left to right orientated body with several thinner branches going in both vertical as well as horizontal direction.
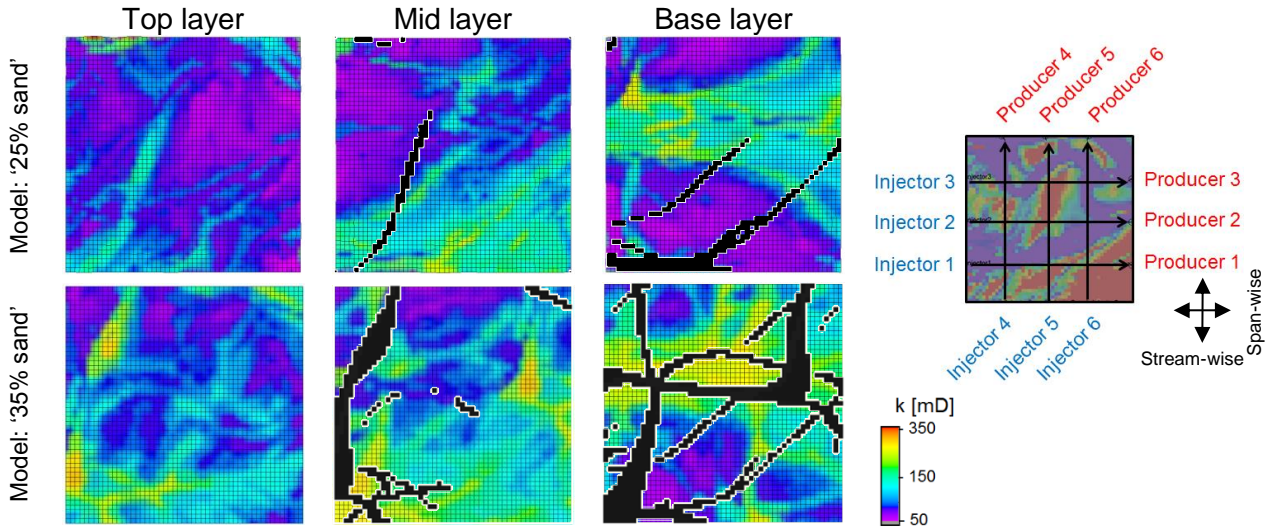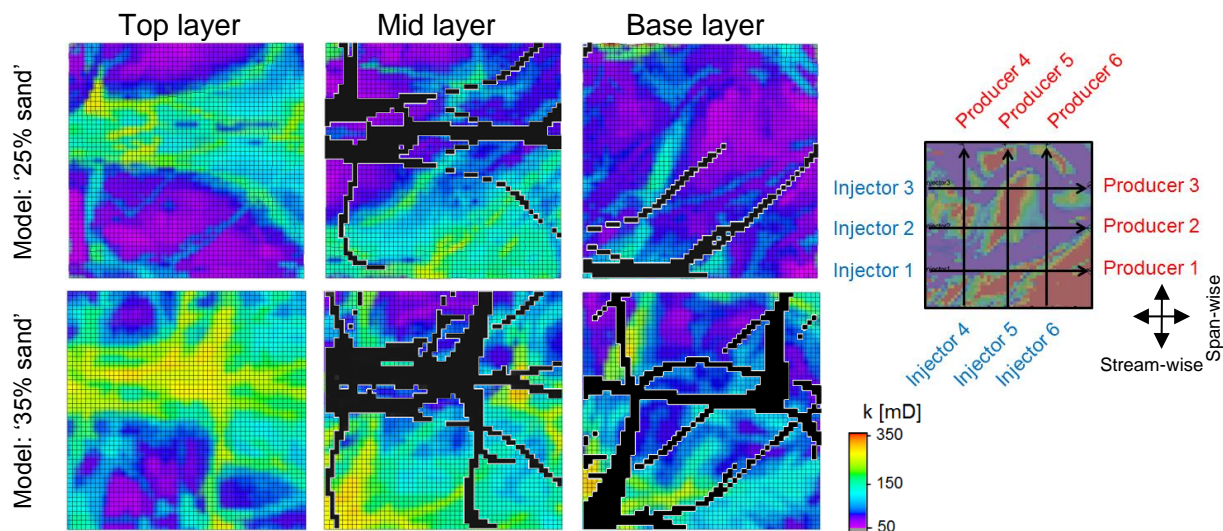
Figure 35: Parasequence-averaged permeabilities for the progradational setting. Black grid blocks symbolize areas of incision of the above-lying layer

Sweep of individual parasequences

The sweep efficiency of the '25% sand' model with a stream-wise well orientation shows values of 19-28% for the base layer and 25-28% for the mid layer (see Figure 36). The difference between the base and the mid layer is between 0-2% for the well doublets 2 and 3 and 5 for the well doublet 1. The sweep efficiency of the top layer is lower than base and mid layer and ranges between the values 19-22%

In the '25% sand' model with a span-wise well orientation the base layer sweep efficiency is 26-28%. The sweep efficiency of the mid layer is 20-24% and for the top layer 13-17%. The difference between the sweep efficiency per layer is reduced by 3-8% going from base layer to mid layer and from mid layer to the top layer.

The sweep efficiency of the '35% sand' model show for the base layer values varying from 31-35%. The mid layer results in values of 24-28% and the base layer of 18-21%. The difference between the sweep efficiency of the base layer and the top layer results in all three simulations in a value of 14%.

In a span-wise orientation of the '35% sand' model the sweep efficiency of the base layer is 28-31% and the top layer is 12-17%. Compared to the stream-wise well pattern of the '35% sand' model, the values reduced by 3-5%. The sweep efficiency of the mid layer is 23-25%.
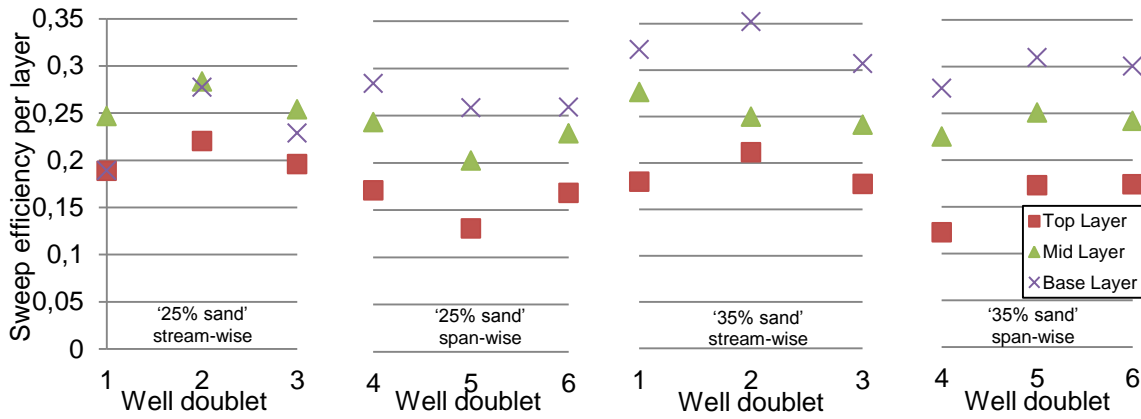
Figure 36: Sweep efficiency for each of the three parasequences in the progradational setting at the end of the simulation (t=50 years)

4.4. Time of water breakthrough and oil peak production flow rate

The peak production rates and the water breakthrough of all models were used to combine the outcomes of all synthetic reservoir models. With the production data available from each simulation it was possible to plot the time of arrival of the first injection water at the producing well against the oil peak production rate before the start of the decline of the production well (see Figure 37).

Stream-wise well orientations for the '35% sand' model cluster in a group of high peak oil productions (200 – 270 m^3/day) and early water-breakthrough (22 - 25 years). The simulations in the '25% sand' model with a stream-wise well orientation cluster in an area with a later time of breakthrough (28-32 years) and a lower peak oil production (120-190 m^3/day) compared to the '35% sand' model.

Span-wise well orientation of the '35% sand' model result in similar peak oil productions (100 – 200 m^3/day) and arrival of injection water at the production well (25 – 35 years) as the stream-wise '25% sand' model simulation. The lowest oil peak production rate (100-150 m^3/day) and the highest time of water breakthrough are reached at the span-wise '25% sand model'.

The '35% sand' model shows the closest proximity to the domain 'high peak production rate - timing of water-breakthrough'. The '25% sand' model with stream-wise orientations situated approximately at the same location where the span-wise '35% sand' values plot. The span-wise orientated wells in the '25% sand' model have the latest water breakthrough and lowest peak oil production with an outlier with a peak oil production of 100 m^3/day at a time of break-through of 42 years.
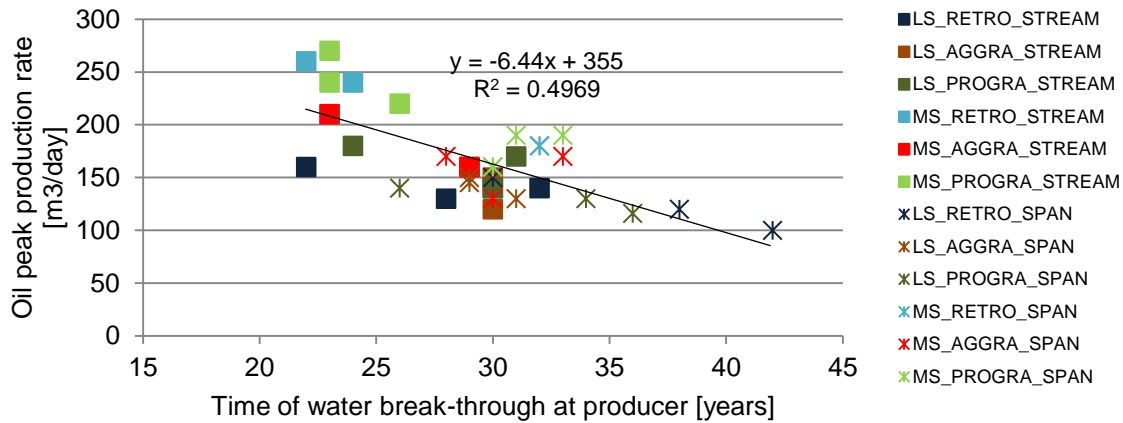
Figure 37: Model comparison of time of first arrival of injected water at the production well against maximum peak oil production. LS = '25% sand' model, MS = '35% sand' model

From the production rate against time the moment in time can be determined where a water cut of 50% is reached. This point is located where the production rate of oil and water intersect. The cumulative water injection volume up to that point was divided by the effective porosity from the given reservoir model to calculate the pore volume injected. This value was plotted against the cumulative oil production which was reached up to this point (see Figure 38). A linear relationship between the pore volume injected and the cumulative oil production between all the models is visible. A cluster is located between 0.3 and 0.4 pore volume of water injected that lead to a water cut of 50 % at the producer. In that time a cumulative oil production between 2 x10^6 and 2.5 x10^6 m^3 is reached. '35% sand delta' model results show a trend to higher pore volume injection and higher cumulative production rate.
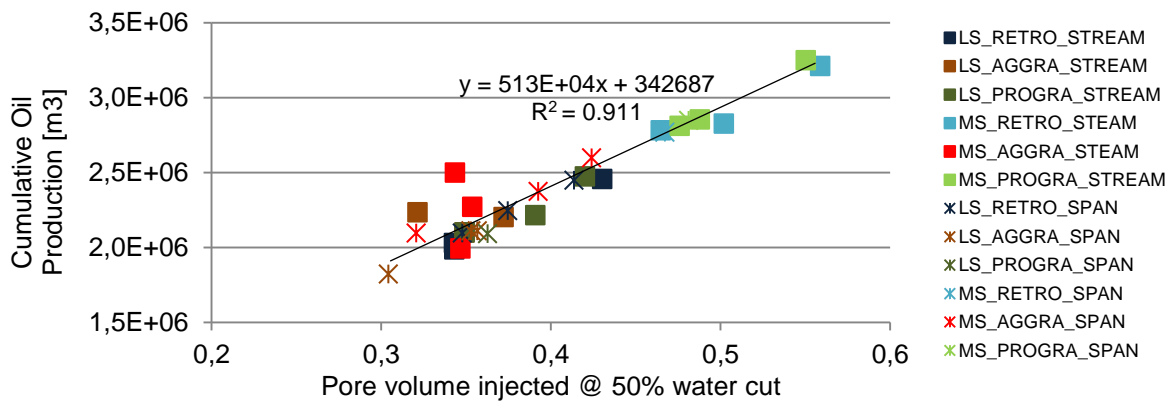
Figure 38: Model comparison of pore volume of water injected until a water cut of 50% is reached against the cumulative oil production at that moment. LS = '25% sand' model, MS = '35% sand' model

Compared to the data of time of water breakthrough against production peak oil rate (Figure 37), the plot of pore volume of water at 50% water cut against cumulative oil production (Figure 38) shows a higher fit to the linear regression (R^2 = 0.911) compared to the previous plot (R^2 = 0.4969).

4.5. Impact of fractures on the flow simulation

The '25% sand' retrogradation model was selected to test the effects of unit confined fractures which have been modelled for this study. The model was chosen because channel incision occurs only in limited areas and the vertical reservoir connectivity in that model is rather low. Therefore the effect of fractures was the most significant for enhancing the reservoir connectivity. Two synthetic reservoir models were created. one has a fracture orientation in the stream-wise and one a fracture orientation in the span-wise direction. First the flow response of the two fractured reservoir models is presented and then the sweep efficiencies for all the layers. The results for the '25% sand' retrogradational model are presented in the same plots as the results of the fractured simulations to make a direct comparison between fractured and non-fractured reservoir models possible.

Flow response analysis

The flow rates over time shows minor differences between the flow model with stream-wise fracture orientation (parallel to the river stream) and the model without fractures (see Figure 39 A - B). The peak oil production for the reservoir model with stream-wise fracture orientation is increased for the well pairs in a stream-wise direction (A) by 0-10% (average: 5%). Towards the end of the simulation the oil production rates in the well doublets 2 and 3 for the stream-wise fractured reservoir intersects with the production rates of the same well pairs for the non-fractured reservoir. The timing of the initial water breakthrough is not changed between the stream-wise fractured model and the non-fractured model for two simulation and for the third the initial water breakthrough is delayed by 0.5-1 year.

The flow rates through the stream-wise fractured reservoir model with the span-wise orientated wells (well doublet 4-6) also show an increased peak production compared to the non-fractured reservoir (Figure 39 B). The peak production rates are increased by 1-8% (average: 4%). The well response of well pair 5 shows an extended plateau rate production of 5 years for the stream-wise fractured reservoir in comparison to the non-fractured reservoir.
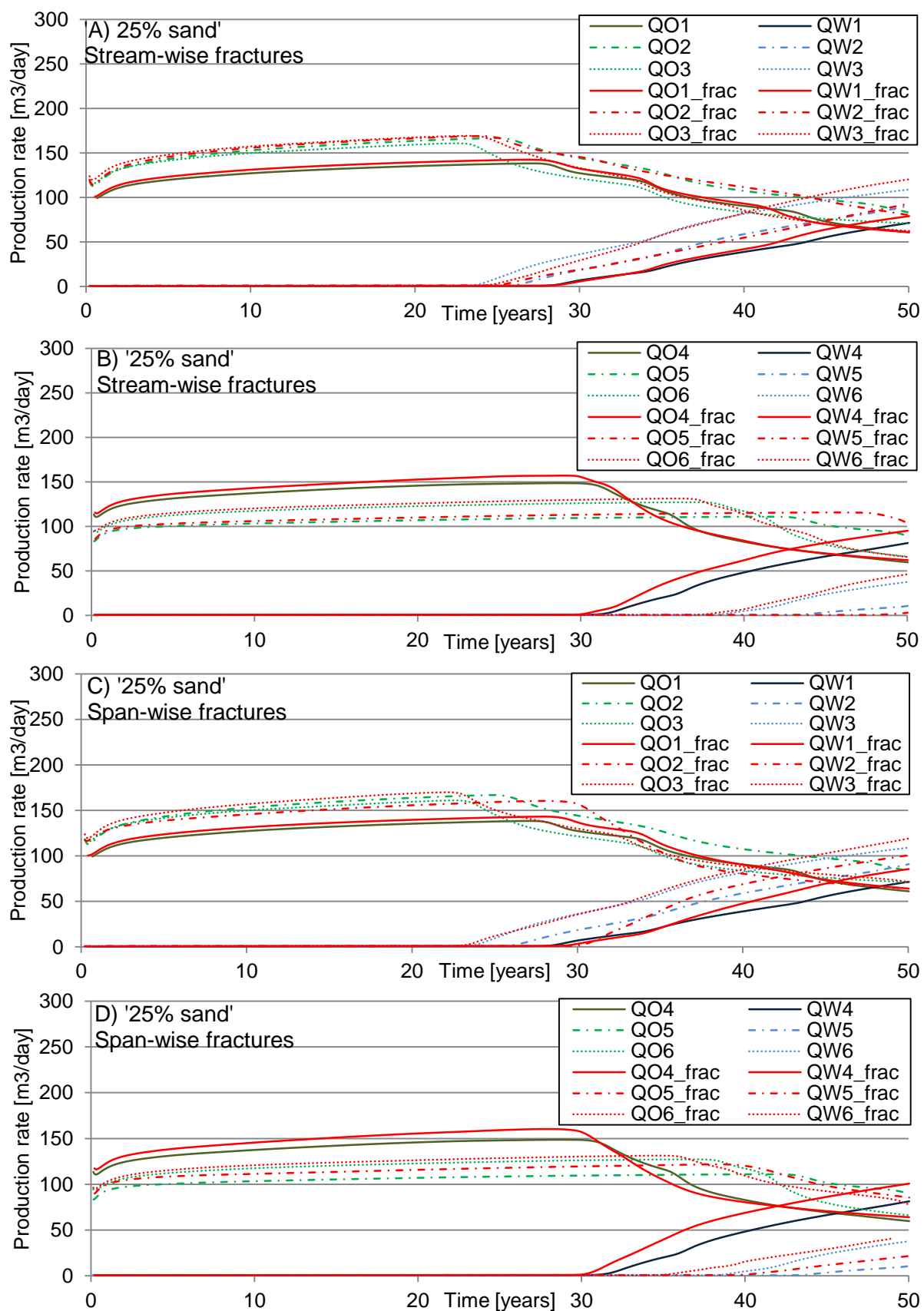
Figure 39: Flow response analysis of fractured '25% sand' model with retrogradational stacking (greenish graphs without fractures - red graphs with fractures)

The flow rate over time shows minor differences for the well pairs 1-3 of the reservoir model with a span-wise fracture orientation (see Figure 39 C –D). The peak production rates are increased by 4% for the well doublets 1 and 3 compared to the non-fractured model. The timing of water breakthrough is the same for the models. The well doublet 2 reaches an equal peak rate oil production as the non-fractured reservoir. However, the timing of water breakthrough is delayed by 4 years which means an extended plateau of15% compared to non-fractured reservoir. After the water breakthrough the oil production curve for the fractured reservoir decrease sharper than the non –fractured model which leads to a higher water cut by the end of the simulation.

Analysis of average permeability maps

The average permeability maps for each of the parasequences for the three reservoir models (non-fractured, stream-wise fractured & span-wise fractured) are presented here (see Figure 40). The maps for the non-fractured reservoir show a high permeable zone in the base layer which becomes wider from the left to the right side of the model. The layer is partly incised by in the lower part by the mid layer. Permeable zones in the mid layer are mainly focussed in the bottom part of the model. In the upper part more patchy permeable zones are present. The top layer has the lowest sand content and thus the lowest permeability. Moderate permeability values are present in elongated zones with a span-wise to diagonal orientation. A channel incision with a width between 50-100m from top to base layer is present at the bottom part of the parasequence.

The average permeability maps for the reservoir model with a span-wise fracture orientation show a high concentration of unit-confined fractures (indicated in red) along the high permeable zone in the base layer. At the flanks at the upper and lower part of the base parasequence where the permeabilites are low, fractures become sparse. Also in the case of the model with the stream-wise fracture network, the fractures are concentrated along the high permeable zone in the middle of the base layer. Fractures which are crossing the entire reservoir model from the base to top are shown in black. In the mid layer unit-confined fractures cover large parts of the parasequence. In the stream-wise fractured case less fractures occur because a high number of intersecting fractures are modelled during the stochastic implementation. These fractures are needed in smaller quantities to reach the modelled boundary of the given fracture area/reservoir volume). In the top layer large areas are covered by unit-confined fractures.
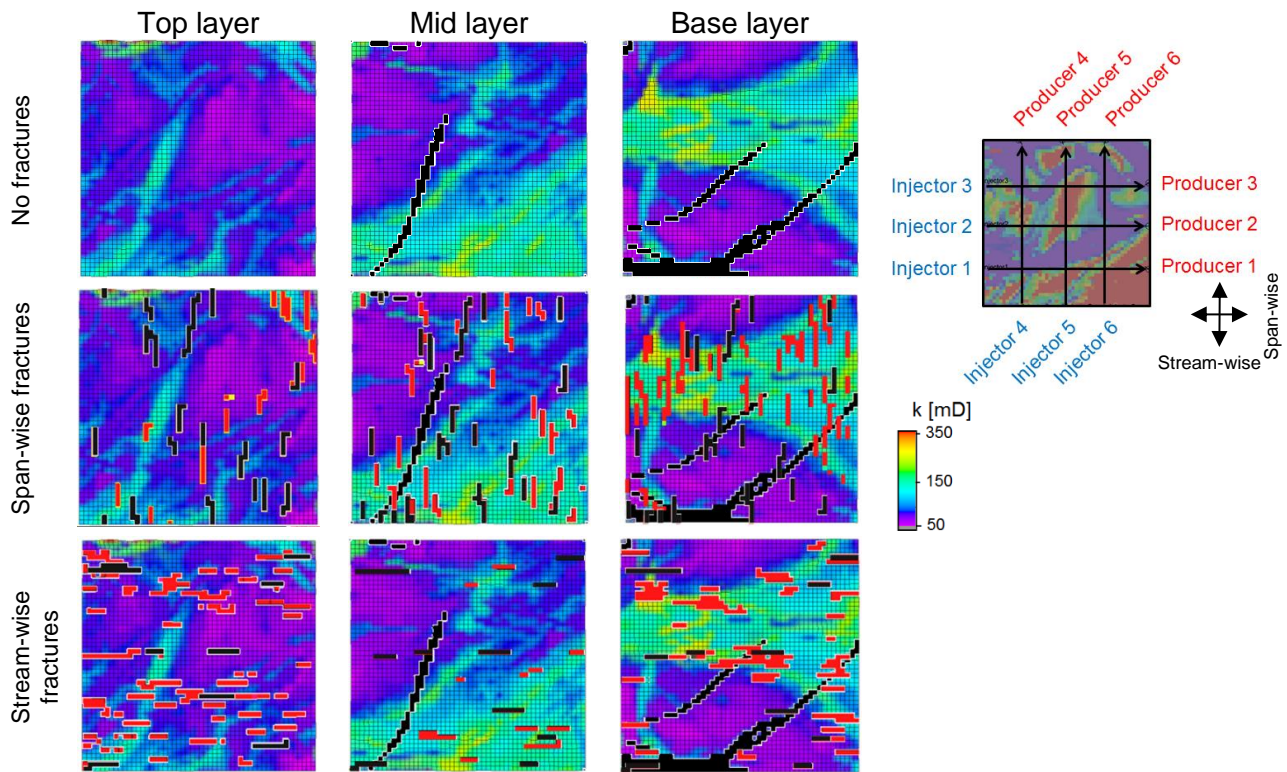
Figure 40: Average permeability maps of fractured '25% sand' model with retrogradational stacking. Upscaled unit confined fractures per parasequence (red) and non-trunctated intersecting fractures (black) are shown.

Sweep of individual parasequences

The comparison between the sweep efficiencies per individual parasequence for the non-fractured reservoir model and the model with the two fracture networks is presented here (see Figure 41).

The sweep efficiency for the well doublets in a steam-wise direction (well doublet 1-3) show little variations between the non-fractured results and the results from the stream-wise fracture network. The variations are in the range of 1% for all parasequences. However, the results from the span-wise fracture network show higher differences compared to the non-fractured results. The sweep efficiency for the base layer is increased for the span-wise fractured model by 2-3%. The mid layer sweep efficiency does not change but the top layer sweep efficiency is decreased for the span-wise fractured model by 1-3% compared to the non-fractured model.

For the wells which are orientated in a span-wise direction (well doublet 4 – 6) both sets of fracture orientations have a significant effect on the sweep efficiency of the individual parasequences. In the initial non-fractured case, the sweep efficiency is narrowly distributed over the three layers in the range of 20-25%. In both fracture cases, the sweep efficiency

improves for the base layer and decreases for the top layer. In the stream-wise fractured model the sweep efficiency of the base layer is 24-27% and for the span-wise fractured model it is 26-28%. The mid layer is increased for the fractured models by 0-3%. The top layer for the stream-wise fractured model has sweep efficiencies of 16-22% which is on average 4% below the non-fractured model. In the span-wise fractured case the sweep efficiency of the top layer is 14-19% which is on average 5% below the non-fractured case.
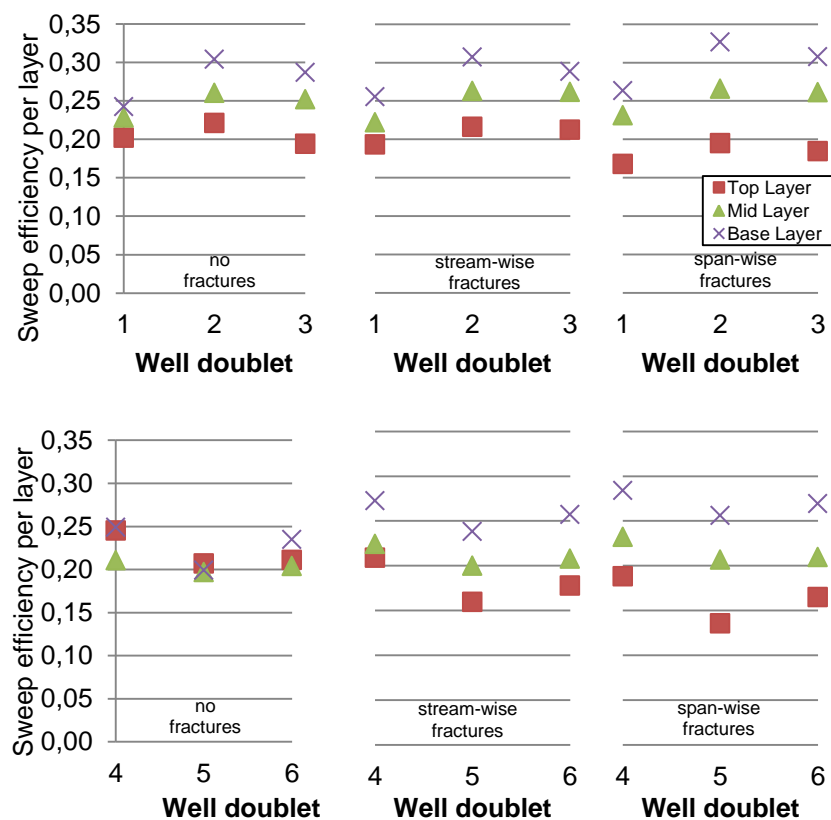
Figure 41: Sweep efficiencies of fractured '25% sand' model with retrogradational stacking pattern.

5. Discussion

This study investigates the potential of process-based numerical Delft3D models as dynamic flow models. The first part of the research was dedicated to the development of a work flow that provides the basis for further analysis of the flow response of Delft3D models. In forms a basis for further investigations of Delft3D models as dynamic flow simulation.

In the second part of the research a case study was investigated as a proof the concept and potential of Delft3D models in flow simulations. Various parameters which potentially have an effect on the flow response were investigated, each addressing a different aspect of the workflow. 8 synthetic reservoir models and a total number of 48 simulation runs were generated. The studied parameters include the input sediment composition of the river (Delft3D), the sequence stratigraphic stacking pattern (Post processing of Delft3D data), the orientation of production and injection wells with respect to the reservoir (Eclipse) and the effect of unit-confined fractures (fracture modelling). The combination of these individual analyses has culminated in proof of concept for the whole workflow.

5.1. Effect of sediment input composition on the reservoir performance

The two different Delft3D models which were used in this study show significant differences in the flow behaviour which can be correlated to their different sediment input conditions. The different sediment compositions results in divergent average permeability maps of the two Delft3D models (e.g. Figure 29).

The incision of overlying parasequences is much more frequent in the '35% sand' model compared to the '25% sand' model as can be seen on the average permeability maps of each of the synthetic reservoir models. The incision leads to a better connectivity of the parasequences. The reason for the more incisions to be occurring in the '35% sand' model could be explained with respect to the observations that were made in the literature.

From Delft3D delta simulations it was concluded that hydraulic and sedimentary forcing mechanisms have a strong effect on the delta morphology. It was concluded that delta with a higher percentage of finer grained (cohesive) sediment input tends to form rather single channels with a higher depth compared to deltas with a higher percentage of coarser grained (non-cohesive) sediment input which leads to multiple channels with less depth (Geleynse et al., 2010) (Caldwell & Edmonds, 2013). In this study, the incision of individual parasequences into each other was modelled in a way that the true depth of incision was

neglected. Incisions that exceed a depth of 1.5 m were set to 1.5 m (or 5 grid blocks). Therefore, no difference in the final dynamic flow models can be observed with respect to the depth of incision. In both the '25% sand' model as well as '35% sand' model the depth of incision is equal. However, the observation that was made it the literature that coarser grained input lead to a higher number of distributary channels is likely to be the main reason why the area of incision is higher in the '35% sand' model compared to the '25% sand' model. The '35% sand' model has formed more channels with a lower depth and has due to the depth incision simplification more incision.

The permeabilities of the '35% sand' models are on average higher compared to the '25% sand' models. This correlation is expected because of the formula applied for the calculation of permeability which is coupled to the mean grain size of sediment (see 3.4 Reservoir Property determination). The permeability average maps show that in the '35% sand' model the permeability values are not only higher but also better distributed over each of the parasequences. This observation could explain why flow simulations in the '35% sand' model exhibit a well-distributed sweep efficiency over the three parasequences since the fluid displacement occurs within a more homogeneous reservoir model than in the '25% sand' models case. However, the results showed the contrary between the two Delft3D models. Different than expected, the '25% sand' model led to a more balanced sweep efficiency over the three separated parasequences compared to the '35% sand' model. Especially the base layer of the '35% sand' model shows in all three stacking patterns (aggradation, retrogradation, progradaton) a much higher sweep efficiency than the mid and top layer. This has a negative effect on the reservoir performance on a long term because the early break-through of water in one layer leads to an increased water-cut of the production well although the other parasequences are still saturated with oil. An explanation for that behaviour could be that gravitational forces lead to a preferential path way of water at the base of the reservoir model. This argument is supported by the results of the progradational stacked models. Here, the base layer has the lowest permeability of the three parasequences and only isolated lenses of permeable zones. Therefore it can be expected that the sweep efficiency through that layer is only limited. Nevertheless, the base layer shows the highest sweep efficiency of all the three parasequences, influenced by the water pushing downwards through the reservoir model. The average permeability maps show that incisions occur over a smaller area in the '25% sand' model compared to the '35% sand' model. Therefore, the water which was initially injected in the top layer has less fluid path ways through which it can migrate downwards during the simulation and hence the overall sweep efficiency is better distributed over the individual parasequences (see Figure 42). The effect of gravitational separation is also a result of the flat grid cell dimension with side lengths of 50m x 50m over

a height of 0.3m. Over these distances the water tends to move though the lower lying layers by gravitational forces.
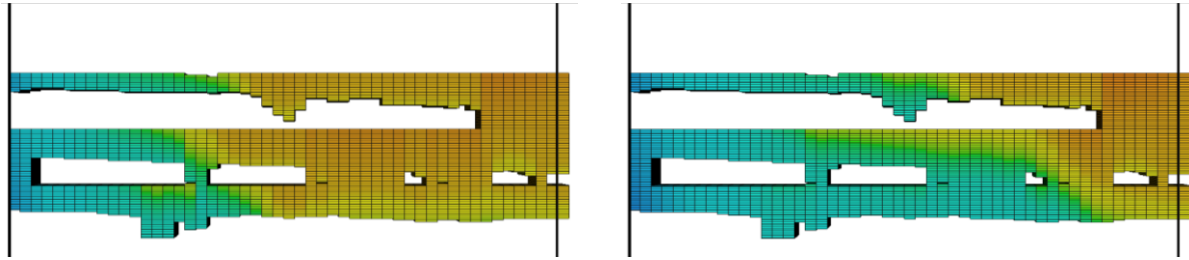
Figure 42: Migration of water (blue) through the dynamic model. 10 years after begin of simulation (left) and 20 years after begin of simulation (right)

The effect of sediment composition on reservoir performance in these synthetic models is summarized as follows

1) Production wells in a deltaic reservoir with a sand input of 35% can produce at approximately 60% higher rates compared to a deltaic reservoir model with a sand input of 25% while the time of water breakthrough is reduced by 20%
2) A reservoir with a coarser sediment input has a higher risk of early water breakthrough through the base layer due to gravitational forces and increased inter-parasequence connectivity
3) Less sand in the input leads to decreased flow performance but a more evenly distributed flow

5.2. Comparison of fluid-flow simulation with stacking pattern

In this study, the flow performance was compared between synthetic reservoir models with varying stacking patterns. Although the individual parasequences are the same in the progradtional and retrogradational flow simulation (but in a reversed order), the flow response show significant differences between these two models.

The permeability average maps of the progradational stacking pattern (Figure 35) show a larger area of incision compared to the permeability average maps of the retrogradational stacking pattern (Figure 32) in both the '25% sand' and the '35% sand' model. In the progradational stacking the channel density increases going upward in stratigraphy. Hence also the area of incision increases which leads to higher vertical permeabilities over the parasequences.

This increased vertical permeability over the parasequences in the progradational stacking leads to a higher dispersion of sweep efficiency of individual parasequences compared to the

retrogradational stacking (Figure 36 & Figure 33). In the synthetic reservoir model with a retrogradational stacking, the sweep efficiencies of the three parasequences show a smaller dispersion mostly in the range of 5% between the highest and lowest value, compared to the progradational stacking which often exceeds 10%. These results indicate that the stacking pattern is an important parameter that has an impact on the flow response of a reservoir model and that a progradational stacking pattern tends to result in higher vertical permeability over parasequences compared to an retrogradational stacking pattern.

With respect to the model comparison graphs, only small differences can be observed between the progradational results and the retrogradational results compared to the effect of different sediment input conditions ('25% sand' and '35% sand' model). The different sediment input conditions clearly result in different clusters on the 'water breakthrough at the producer' against the 'oil peak production rate' plot (Figure 37). Hence the '35% sand' model results cluster at high peak oil rates and an early water breakthrough whereas the simulations of the '25% sand' model have lower peak oil productions and a later water breakthrough. Different than the sediment input conditions, the stacking pattern does not lead to such a clear separation of simulation results. Instead, the simulation results of related well pairs (e.g. '35% sand' model, progradational stacking, well pairs 1-3 'stream-wise') show a high variability among themselves which indicates that the location of the well placement has a strong effect on the flow performance of the reservoir. Therefore the location of a channel (or a zone of higher permeabilities) can highly influence the performance of a well doublet.

One simulation run with the '35% sand' model in the aggradational stacking shows a different flow behaviour with a peak production flow rate more than 50% higher than the two adjacent wells with the same orientation (see Figure 28 C). The dynamic 3D grid was examined in order to find indications that would lead to such a high deviation and a much higher peak oil production (see Figure 43). The reservoir produced from the three parasequences individually with the well pair 1 and well pair 3. In the well location of well pair 2 the reservoir was penetrated in a location with a local incision of the middle parasequence into the lowermost sequence. This leads to a better connection of permeable reservoir unit to the injection well which consequently leads to a better communication of the injection and production well. Additionally, in between the top and middle parasequence another incision occurs in the distance away from the injectors at the well location of well pair 2. That leads to an enhanced communication of the producer 2 to the reservoir units. This results in a much higher production flow rate and an earlier water breakthrough.
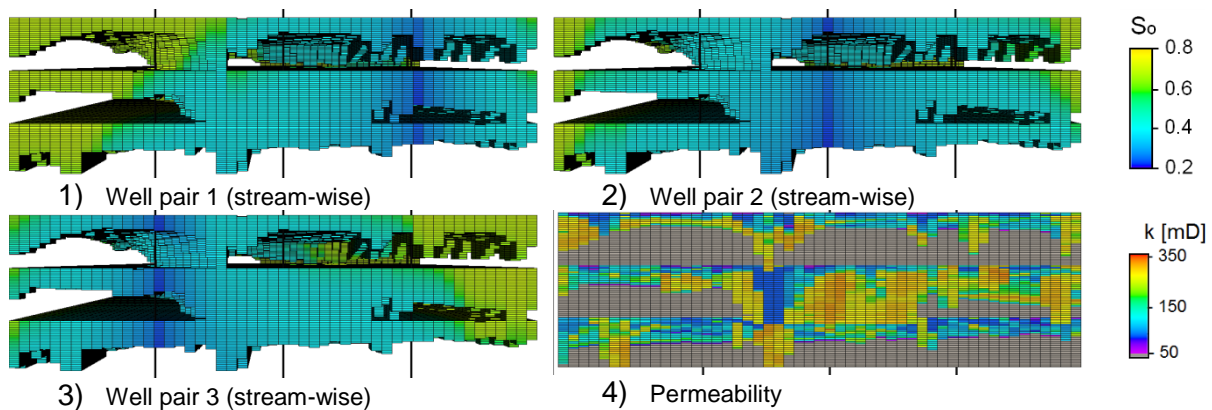
Figure 43: Vertical cross section along the injector side of the simulation. 1 – 3: oil saturation after 20 years. Black vertical lines are injectors 4: permeability distribution

The given example shows how strong the position of the well placement can influence the flow response of the reservoir model. Due to the localized channel the flow response becomes very different compared to the related two well doublets. The difference is much higher than the variances observed when comparing flow simulations with different stacking patterns.

This observation raises the question about the relative importance of both the large scale stacking trend and the localized occurrence of channels on the flow performance of a reservoir. In the literature it is stated that stacking patterns of delta lobes are both controlled by autogenic (channel avulsion) and allogenic control factors (relative sea level rise and sediment supply) (Wellner, 2005) which can result in a offset of direction of two successive deltas lobes in angles as high as 90˚ in both clockwise and anticlockwise direction (Deveugle et al., 2011). Due to these dynamics of the delta system it is important to recognize that the sedimentary succession are unlikely to form a clear stacking trend of a progradational or retrogradational sequence. It shows that on a small scale of three parasequences (as in the model setup of this study) the importance of conventional sequence stratigraphic terms such as progradation and aggradation is highly dependent on the heterogeneity of the individual parasequences governed by the presence of channels in the system.

A practical approach from the literature was presented in this study that provides a differentiation of systems tracts in deltaic sediments by using the sand content over parasequences described in sediment cores and well logs (Ainsworth et al., 2011). Their technique can be used to determine a stacking pattern from real reservoir data which subsequently can be used to create a process-based reservoir model of a real reservoir. The process-based models provide a more realistic tool on the view of the potential heterogeneity of a deltaic sequences compared to many other, mostly stochastically-driven reservoir modelling techniques.

The sweep efficiencies per layer show significant differences for the aggradational model between the '25% sand' model and the '35% sand model. In the '25% sand delta' model none of the three parasequences are very dominant in terms of big channels and higher average permeability. Incisions occur from top to mid and mid to base layer in a south-west to north-east trend. That distribution of reservoir properties over the three parasequences leads to a well-distributed flow over the entire flow model. In contrast, the sweep efficiency in the '35% sand delta' model shows a higher difference between the base and the other two layers. This discrepancy can be explained with the high permeability values of the base layer in combination with the high degree of incision of the mid layer into the base layer. These two parameters lead to a preferential flow path through the base layer of the synthetic reservoir model. The top layer in the span-wise well orientation is fairly isolated and incises only at limited locations into the mid sequence.

The effect of stacking pattern on reservoir performance in these synthetic models is summarized as follows:

1) A progradational stacking pattern results in higher area of incision than retrogradational stacking pattern and hence increases the vertical permeability
2) Because of the increased vertical permeability in the progradational stacked model, the sweep efficiencies of individual parasequences is more dispersed and early water breakthrough more probable
3) Local occurrence of channels at the well location have a stronger effect on the reservoir performance than the general stacking pattern

Improving the stacking of parasequences

In vicinity of channel deposits the topographic differences become very large and an incision into lower lying strata is probable. When the topographic information is neglected, the positioning of grid cells in the model is erroneous. At locations with high topographic changes (especially channels) the grid cells are modelled much shallower than they actually occur. Also the banks of the channels are affected by that disregard.

One way to incorporate the final topography of the Delft3D parasequences is by shifting the grid vertically at each horizontal grid point to follow the topography (see Figure 44). This allows the incision of the channels to be represented closer to the original output of the Delft3D models. The downside here is that related flow units are disconnected by the vertical incremental movement of the grid cells. This means that grid cells which initially are in communication become separated from each other through the incremental displacement. Because of that this approach was not applied in this study.
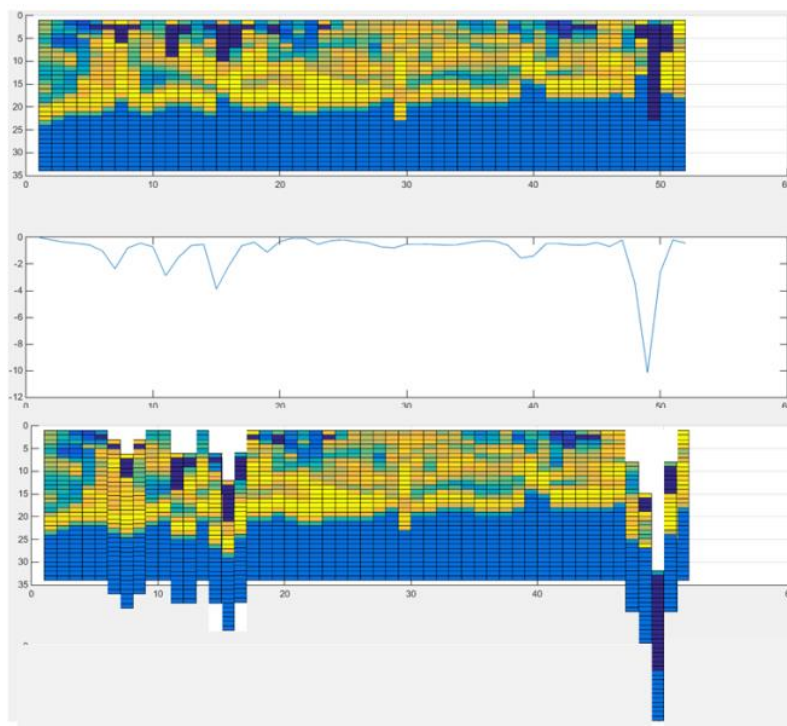
Figure 44: 2D vertical cross section of a Delft3D model. Matrix of the 'f_b'-file (top), topography 'z_b'-file (middle) and incremental change from 'f_b'-file according to 'z_b'-data (bottom)

5.3. Effects of well placement strategy on reservoir performance

The simulations that were conducted in this study always consisted of 6 flow simulations per model. The results have shown that the flow response is highly influenced by the location where the injector and producer are located. In cases where the wells penetrate the synthetic reservoir model where incision of the parasequences occurs the flow response becomes much different, namely with a high peak production and an early water-breakthrough. This shows that the number of simulations per reservoir model should be increased to reach a better distinction between simulation results that were governed by a high Net/Gross ratio and vertical connectivity and those which penetrate the reservoir model at isolated parasequences. Also, only stream-wise and span-wise well pairs with a fixed distance of 2.5km were used to investigate the flow behaviour of the synthetic reservoir models. Diagonal well arrangements and varying producer-injector distances would give the analysis of the flow response of the models a further dimension. A strategy for the well placements which was developed for this study is presented below (Figure 45). However, it was not applied in this research since the results from 48 simulations already created sufficient data to proof the concept of feasibility.

6x 2.5 km

6 x 2.6 km (diagonal)

8 x 1.8 km

12 x 1.25 km

8 x 800 m (diagonal)
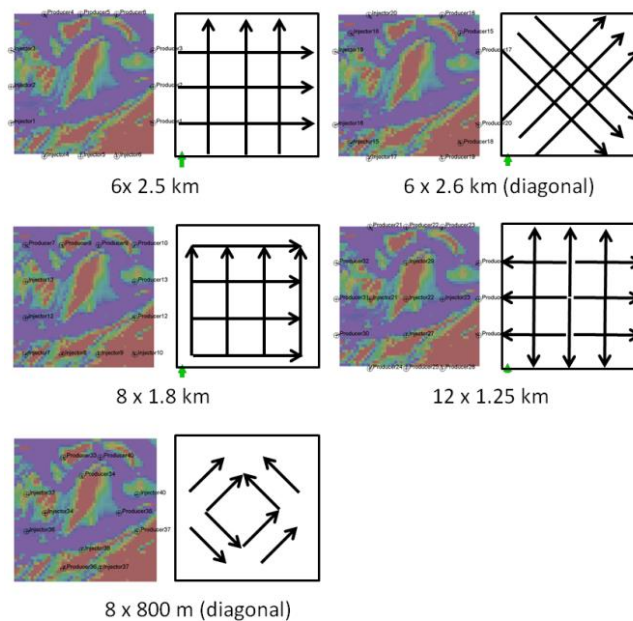
Figure 45: Overview of additional well spacings

5.4. Effects of fractures

The '25% sand' model with a retrogradational stacking pattern was used to study the effect of unit-confined fractures. Two different fracture networks were integrated into the reservoir model of which one has a fracture orientation in a stream-wise direction and one with a fracture orientation in a span-wise direction. The results of the flow simulations were compared with the results of the non-fractured reservoir. The comparison was made with the results of the dynamic flow analysis, the average permeability maps and the sweep efficiency per layer.

The flow rates over time do not vary greatly between the non-fractured and fractured models. On average the oil peak flow rate is increased by 4-5%. These results indicate that the injector-producer connectivity is improved by the added fractures to the system. Moreover, the average permeability maps show that multiple fractures are present over the entire height of the reservoir model which indicates that the individual parasequences are in closer communication. The increased peak oil rate lead to less pressure needed to operate the reservoir at a certain performance which means from an economic view point of view that the reservoir performance is improved.

However, the increased peak oil rate and enhanced reservoir connectivity is not necessarily beneficial for the long term performance of the reservoir. The trends of the oil rate production of the fractured models intersect with the rates of the non-fractured reservoir in approximately 5 years after water breakthrough. From that point on, the production rates of the non-fractured reservoirs are higher. Another key observation which suggests that fractures might also reduce the performance of a reservoir is by looking at the sweep efficiencies per parasequence. The results show that fractures lead to a higher dispersion of the individual sweep efficiencies. In an optimal case, the sweep efficiency is constant over all the layers. If so, the water front moves with a constant velocity over each of the parasequences. If the difference is high between individual parasequences, an early water break-through in one layer can cause the well to be closed due to a high water-cut despite the fact that adjacent parasequences are still oil-prone. The sweep efficiency results show that the base layer is swept more efficiently compared to the mid and especially the top layer. It is likely that the improved vertical connectivity which is induced by the fractures reduces the efficiency of the top layer because of gravitational forces. The water which is pumped into the formation at the injection well is in the beginning distributed almost equally over the three parasequences. While the water migrates towards the production well and replaces the oil pore fill with water, more and more water migrates towards the base of the reservoir through the improved vertical connectivity. By the time the water front reaches the production well at

the base layer, it is far behind in the top layer. Continuing the production would eventually also sweep the top layer, but the costs of running the pumps is will impact economic considerations.

The average permeability maps show the behaviour of unit confined fractures as they were described and quantified by researchers in outcrop studies. First of all, the fractures on the permeability maps show a concentration of fractures in the locations with higher permeability values because they also represent rocks with a more brittle mechanical behaviour. In contrast to that low permeable rocks have a more ductile mechanical behaviour. This fracture concentration can be observed the best in the base layer of the two fractured models. Moreover, the average permeability maps also show a correlation of fracture spacing distance over bed thickness. As other studies suggest, the fracture density decreases with increasing thickness of a bed (e.g. Bertotti et al., 2007 and references therein). The fracture implementation method developed for this study shows the same trend. This is because the fracture intensity in this approach is defined as the P32 (total surface area of fractures / volume of rock mass). Therefore thinner brittle mechanical beds need a higher number of fractures since the truncation at top and base of the mechanical unit results in small fracture surface areas than a thick layer with fractures with big surface areas.

The orientation of the fracture network with respect to the main trend of delta migration shows differences in the flow performance. The sweep efficiencies show higher variations for the fracture network which is orientated in a span-wise direction than in a stream-wise direction. The span-wise fracture network leads to breakage of the lithologies in a direction which lies perpendicular to the main flow direction. The geometry of geobodies (zones with higher permeability) is often orientated from the river channel towards the offshore, or in other words in a stream–wise direction. In reality a succession of deltaic parasequences does not necessarily form a stack of deposits with the same orientation of permeable zones. Large scale avulsions cause the source to shift and reorient which leads to varying orientations of geobodies in the geological record. Therefore it should be considered to be an approximation whether a fracture pattern is perpendicular or parallel to the depositional trend.

The best example of a parasequence which has an orientation of the permeable zone perpendicular to the fracture pattern of the base layer in the fracture study. It is suggested that the fracture network which is orientated perpendicular to that sedimentological trend does not increase the vertical permeability more than a stream-wise fracture pattern, but that it increases the horizontal permeability between sand bodies, since these form along permeable zones with an elongated stream-wise shape. The average permeability maps

show how span-wise fractures lead to an increased width of permeable connections which improve the reservoir communication.

The terminology of stream-wise and span-wise can also be seen critical with respect to the orientation of the present fracture network. In an ideal case with an active margin with the same orientation as the Delft3D model, meaning a coastline from North to South, it is legitimized to assume that the fracture pattern has an orientation in a span-wise direction, or in other words parallel to the coastline. The largest horizontal stress (tectonic stress) in such a system is likely to be perpendicular to the coastline and the smallest horizontal stress parallel to the coastline, which would also be the orientation of the fractures.

6. Conclusion

This study developed a workflow to use process-based geological models created in Delft3D as synthetic reservoir model in a dynamic flow simulation. The proof of feasibility was successfully demonstrated using two delta distributary networks with varying sediment input conditions. A procedure was applied to convert sediment compositions to reservoir properties such as porosity and permeability. A new technique for the generation of stacked parasequences from Delft3D models was introduced and summarized in a guide that provides a basis for further studies which are related to the topic of sequence stratigraphic stacking of Delft3D models. Different production-injection well doublets were used in this study to investigate the effect of well pair orientation on the flow performance. Moreover, this study also entails coupling of mechanical unit-confined fractures, as they are described in literature, which can be implemented into the dynamic flow simulation.

The results suggest that deltas formed under conditions of a higher sand concentration lead to improved performance of an injection-production well doublet due to higher porosity and permeability values. It also leads to a higher connectivity of parasequences, however this is linked to a risk of early water breakthrough due to gravitational forces acting on the reservoir fluids.

The effect of sequence stratigraphic stacking was investigated by generating synthetic reservoir models with a progradational, aggradational and retrogradational stacking pattern. The results indicate that a prograding deltaic sequence leads to higher vertical connectivity than a retrograding sequence. Hence, sweep efficiencies of individual parasequences in a prograding system are more dispersed than in the retrogradational setting. However, the local existence of channels at the well location has a more dominant impact on the reservoir performance than the stratigraphy when comparing their effect on the reservoir flow performance. Hence it was concluded that understanding the heterogeneity induced by varying channel locations is at least as relevant, if not more relevant, as the understanding the general stacking trend.

It was also demonstrated that the production behaviour is dependent of the orientation of the production-injection well doublet. Moreover, the results give indications that unit-confined fractures can both increase and decrease the productivity of a well doublet, depending on their orientation with respect to the stream direction of the deltaic system and the orientation of the well doublet.

The outcomes of the case study give conceptual results and should be regarded as a proof of concept rather than a deterministic reservoir characterisation.

Future work must focus on understanding the role of channels with respect to different stacking patterns and these can be better predicted from field data. Also, the modelling of the sequence stratigraphic context and the stacking of individual parasequences has to be improved in order to reach a solid geologic succession of deltaic units. This could be done by implementing erosional surfaces and the modelling of lag deposits.

Due to the extensive computer power needed to run the simulations in Delft3D it will most certainly not be possible in the near-future to model an entire reservoir over larger geological times in one model run. Therefore the quantitative research in the form presented in this study will continue to rely on the post-simulation stacking. If however it should be possible to incorporate the entire reservoir in one simulation, it would be an even greater enrichment in the characterization of reservoirs in the subsurface. These models could be run on a bathemetric file, obtained from paleogeographic reconstructions of the given reservoir location which models the depositional phases even more realistically. It might even be possible at some day that large scale tectonic structures such as growth faults are modelled by abrupt displacement of the basin floor during the simulation.

References cited

Aisworth, R. B., Vakarelov, B. K., & Nanson, R. A. (2011). Dynamic spatial and temporal prediction of changes in depositional processes on clastic shorelines: Toward improved subsurface uncertainty reduction and management. *AAPG Bulletin, V.95, No. 2*, 267-297.

Bertotti, G., Hardebol, N., Taal-van Koppen, J., & Luthi, S. (2007). Towards a quantitative definition of mechanical units: New techniques and results from an outcropping deep-water turbidite succession (Tanqua-Karoo Basin, South Africa). *AAPG Bulletin, V. 91, No. 8*, 1085-1098.

Bertotti, G., Immenhauser, A., & Taal-van Koppen, J. (2005). Stratigraphic and regional distribution of fractures in Barremian-Aptian carbonate rocks in eastern Oman: Outcrop data and extrapolation to interior Oman hydrocarbon reservoirs. *International Journal of Earth Sciences, v.15*, 447-461.

Caldwell, R. L., & Edmonds, D. A. (2013). A numerical modeling study of the effects of sediment properties on deltaic processess and morphology. *Journal of Geophysical Research: Earth Surface*.

Cooke, M. L., & Underwood, C. A. (2001). Fracture termination and step-over at bedding interfaces due to frictional slip and interface opening. *Journal of Structural Geology 23*, 223-238.

Cooke, M., Simo, J., Underwood, C., & Rijken, P. (2006). Mechanical stratigraphic controls on fracture patterns within carbonates and implications for groundwater flow. *Sedimentary Geology 184*, 225-239.

Deltares, B. 1. (2011). Retrieved from Delft3D-FLOW-USER-Manual: http://oss.deltares.nl/documents/183920/185723/Delft3D-FLOW_User_Manual.pdf

Dershowitz, B., LaPointe, P., Eiben, T., & Wei, L. (1998). Integration of Discrete Feature Network Methods with Conventional Simulator Approches. *SPE Annual Technical Conference and Exibition* (pp. 351-359). New Orleans, Lousiana, USA: Society of Petroleum Engineers, Inc.

Dershowitz, W., Lapointe, P., & Cladouhos, T. (1998). Derivation of Fracture Spatial Pattern Parameters from Borehole Data. *Int. J. Rock Mech. Min. Sci. Vol. 35, No. 4/5*, (p. 134).

Deveugle, P., Jackson, M., Hampson, G., Farrell, M., Sprague, A., Stewart, J., et al. (2011). Characterization of stratigraphic architecture and its impact on fluid flow in a fluvial-dominated deltaic reservoir analogue: Upper Cretaceous Ferron Sandstone Member, Utah. *AAPG Bulletin, V. 95, No. 5*, 693-727.

Farrell, M., & Abreu, V. (2006). Reservoir connectivity in fluvial-deltaic depositional environments: South Timbalier 26 field study (abs.). *AAPG International Conference and Exhibitions.* Perth, Australia.

Galloway, W. (2008). *Depositional Evolution of the Gulf of Mexico Sedimentary Basin, Sedimentary Basins of the World, Volume 5.* Elsevier B.V.

Galloway, W. G. (1975). Process framework for describing the morphologic and stratigraphic evolution of deltaic depositional systems. *Broussard ML (Ed), Deltas, Models for exploration, 2nd*, 87-98.

Geleynse, N. (2013). On the modelling of river delta formation. *PhD thesis, TU Delft, Applied Earth Sciences, Delft*.

Geleynse, N., Storms, J. E., Walstra, D. J., Jagers, H. R., Wang, Z. B., & Stive, M. J. (2010). Modelling of a mixed-load fluvio-deltaic system. *Earth and Planetary Science Letters 302*, 217-226.

Komar, P. (1973). Computer models of delta growth due to sediment input from rivers and longshore transport. *Geological Society America Bulletin, v. 84*, 2217-2226.

Larue, D., & Legarre, H. (2004). Flow units, connectivity, and reservoir characterization in a wave-dominated deltaic reservoir: Meren reservoir, Nigeria. *AAPG Bulletin, v.88, No.3*, 303-324.

Laubach, S. E., Olson, J. E., & Gross, M. R. (2009). Mechanical and fracture stratigraphy. *AAPG Bulletin, V. 93, No. 11*, 1413-1426.

Leeder, M. (1999). *Sedimentology and Sedimentary Basins, From Turbulence to Tectonics.* 1. Sedimentology, Blackwell Science Ltd.

Makaske, B. (2001). Anastomosing rivers: a review of their classification, origin and sedimentary products. *Earth Science Review 53 (3-4)*, 149-196.

Orton, G., & Reading, H. (1993). Variability of deltaic processes in terms of sediment supply, with particular emphasis on grain size. *Sedimentology, 40*, 475-512.

Panda, M., & Lake, L. W. (1994). Estimation of single-phase permeability from parameters of particle-size distribution. *AAPG Bulletin, V. 78, No. 7*, 1028-1039.

Parney, B., & LaPointe, P. (2002). *Fractures can come into focus*. Retrieved July 30, 2015, from American Association of Petroleum Geologists: https://www2.aapg.org/explorer/geophysical_corner/2002/10gpc.cfm

Postma, G. (1990). An analysis of the variation in delta architecture. *Terra Nova, 2*, 124-130.

Roelvink, J. (2006). Costal morphodynamic evolution techniques. *Costal Engineering, 53(2-3)*, 277-287.

SCHLUMBERGER. (2013). *ECLIPSE Reference Manual Version 2013.2, Technical Description.*

SCHLUMBERGER. (2015). *Petrel E&P Software Platform Version 2013.8.*

Slingerland, R., Burpee, A., & Edmonds, D. (2012). Grain size controls on the facies sequences and clinoforms of river-dominated deltas. *AAPG annual convention and exhibitions*.

Takebayashi, H., & Fujita, M. (2014). Spatial distribution of porosity of bed material, bed strength and size distribution of bed material on bars. *River Flow - Schleiss et al. (Eds).*

The Mathworks Inc., MATLAB Version R2014b. (n.d.). Natick, Massachusetts, United States: The MathWorks Inc.

Tyler, N., & Finley, R. (1991). Architectural controls on the recovery of hydrocarbons from sandstone reservoirs. In A. D. Miall, & N. Tyler, *The three dimensional facies architecture of terrigenous clastic sediments and its implications for hydrocarbon discovery and recovery* (pp. 1-5). SEPM Concepts and Models in Sedimentology and Paleontology.

Van Wagoner, J., Mitchum, R., Campion, K., & Rahmanian, V. (1990). Siliciclastic sequence stratigraphy in well logs, cores, and outcrops: concepts for high-resolution correlation of time and facies. *AAPG Methods in Exploration 7*, 63.

Wellner, R. B. (2005). Jet-plume depositional bodies – The primary building blocks of Wax Lake delta. *Transactions of the Gulf Coast Association of Geological Societies, v. 55*, 867-909.

Wright, L., & Coleman, J. (1973). Variations in morphology of major river deltas as functions of ocean wave and river discharge regimes. *AAPG Bulletin, v. 57*, 370-398.

List of abbreviations

- A/S ratio   Accomodation space/ Sediment supply ratio

- T_h Thickness of individual parasequence

- S/S_h Sand/Shale ratio

- S_O Oil saturation

- MOV   Movable oil volume

- S_{wc} Conate water saturation

- S_{OR} Residual oil saturation

- k   Permeability

- φ Porosity

- D_P D50 grain diameter

- P_{32} Total surface area of fractures/ Volume of rock mass

Appendix

Delft 3D-FLOW model set-up

Grid	Number of grid cells in M-Direction		500				
	Number of grid cells in N-Direction		600				
	Delta X [m]		50				
	Delta Y [m]		50				
	Origin X [m]		0				
	Origin Y [m]		0				
	Rotation left [deg]		0				
Simulation time	Time [days]		180				
	Time step [min]		0,5				
Morphology	Scale factor		50				
	Spin up		20				
	Min. depth		0,1				
	van rijn		1				
	Threshold sediment thickness		0,05				
	Multiplication factors		1				
Boundaries	River:	Total discharge					
		Reflection parameter	500				
		Time Series					
		Discharge [m3/s]	2000				
	North/South:	Neumann, Harmonic					
		Discharge	none				
	Basin:	Water level, Harmonic					
		Reflection parameter	500				
		Frequency [deg/h]	0	13,9	15	28,8	30
		Amplitude [m]	0	0,164	0,221	0,699	0,465
		Phase [deg]	0	130,36	159	276,88	322,6
Physical parameters:							
		Gravity [m/s2]	9,81				
		Water density [kg/m3]	1000				
		Bottom Roughness	Manning	U	0,03	V	0,03
		Viscosity	Uniform	Eddy visc.	1	Eddi diff.	1

Appendix 1: Delft3D-FLOW Model set-up

Top Sequence	Middle Sequence	Base Sequence	
			Average permeability

Saturation grid

t = 10 years

t = 20 years

t = 30 years

t = 40 years
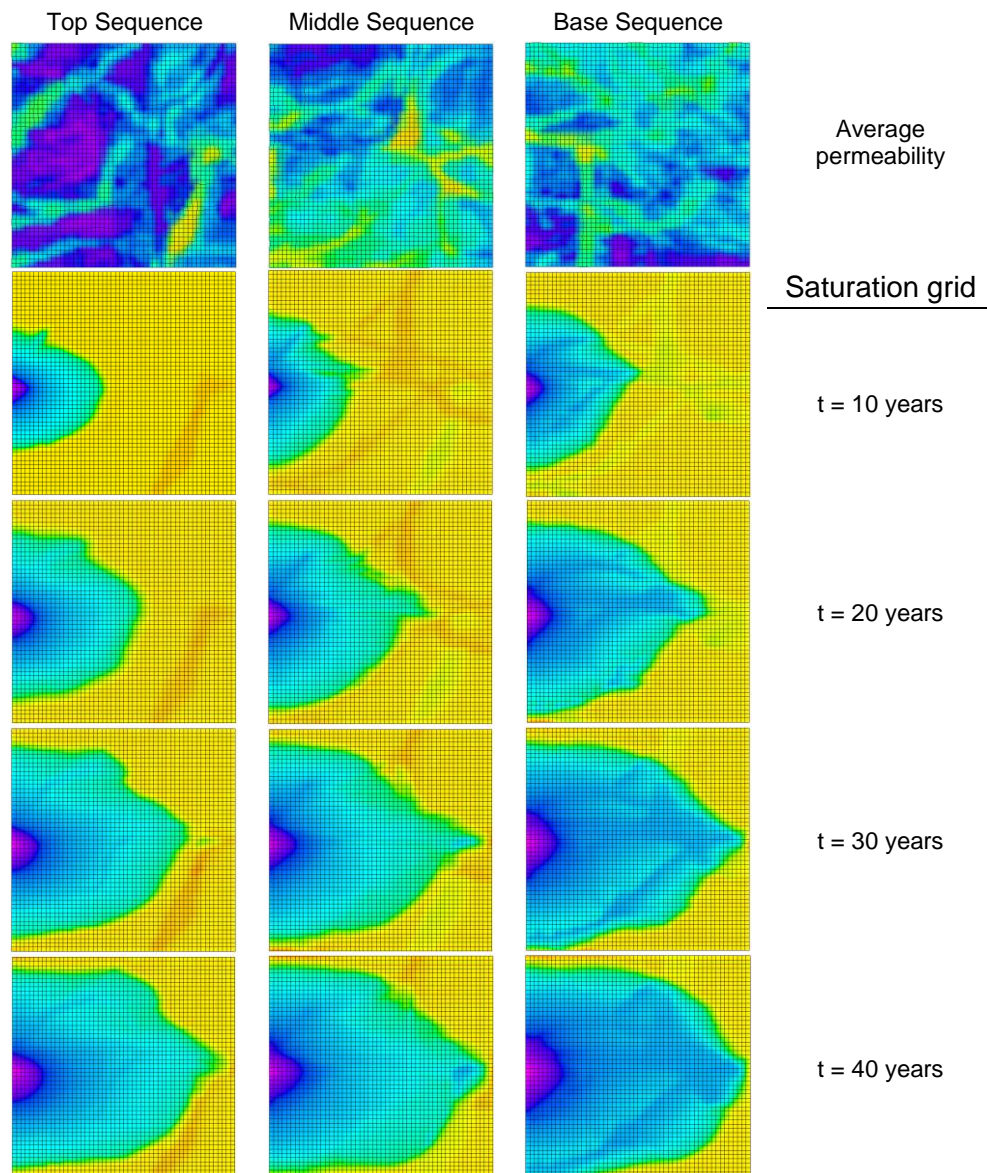
Appendix 2: Dynamic composite results of Delft3D model '35% sand delta', aggradational stacking, well pair 2

Additional technical information for the Eclipse simulation

Corey values for the curves:
Sorw: 0.2, Corey O/W: 3, Kro@Somax: 0.9
Swmin:0.2, Swcr: 0.22, Corey water: 4, Krw@Sorw: 0.8, Krw@S=1
Used Simulator: ECLIPSE 100, Additional adjustments in the Editor:
RUNSPEC
    1) NSTACK
    "NSTACK
    -25 /"
    2) NUPCOL
      "NUPCOL
      8 /"
SCHEDULE
    1) MESSAGES
      "MESSAGES
      6* 100000 6*100000 /